# Convexification approaches for regional route guidance and demand management with generalized MFDs

Charalambos Menelaou, Stelios Timotheou*, Panayiotis Kolios, Christos G. Panayiotou

*KIOS Research and Innovation Center of Excellence, and the Department of Electrical and Computer Engineering, University of Cyprus,*
{menelaou.charalampos, stimo, kolios.panayiotis, christosp}@ucy.ac.cy

**Abstract**

Traffic congestion is one of the main concerns in big cities with many adverse socioeconomic effects. A promising solution is to simultaneously regulate the admission of vehicles (i.e., demand management) and redistribute traffic flows within the network (i.e., route guidance). In this work, we integrate demand management with route guidance within a Model Predictive Control framework using regional traffic dynamics with generalized Macroscopic Fundamental Diagram (MFD) shapes. Dealing with generalized MFD shapes is challenging due to the resulting nonlinear and non-convex optimization formulation. To tackle this challenge, we develop two real-time solution approaches: (i) a successive convexification approach that constructs convex bounding sets for all nonlinear terms, and (ii) a linear approximation approach that solves the problem using triangular macroscopic fundamental diagram approximations. The proposed approaches offer a trade-off between execution speed and solution quality, as the linear approximation approach runs faster while the successive convexification approach yields better quality and accuracy solutions. Macroscopic simulation results illustrate the efficiency of the successive convexification and linear approximation approaches yielding an optimality gap of less than 3.5% and 10% in all considered cases, respectively. Furthermore, both approaches outperform a state-of-practice nonlinear solver in terms of solution quality and execution time. Finally, substantial gains are also obtained regarding travel time and traffic flow efficiency in a realistic microsimulation environment.

*Keywords:* Demand Management, Route Guidance, Intelligent Transportation Systems.

## 1. Introduction

Traffic congestion is one of the most challenging problems that modern cities face causing several societal, health, economic and environmental issues (Arnott and Small, 1994). For this reason, a plethora traffic management strategies have been proposed aiming to control road infrastructure elements (e.g., traffic signals, variable message signs and variable speed limits) or affect the decisions of travellers (e.g., routes to follow, journey departure times) in an effort to alleviate the adverse effects of congestion (Papageorgiou et al., 2003).

One such strategy is *route guidance* in which traffic is redistributed across the non congested areas by suggesting alternative routes to drivers (Papageorgiou, 1990). The majority of route guidance methods were developed utilizing highly-complex, detailed microscopic dynamics that utilize extensive per vehicle-based information about the speed and position (Mahmassani, 1998). Besides, considering microscopic traffic dynamics often results in solution methods that attempt to improve the travel time of individual vehicles, which in turn can negatively affect the overall network efficiency (Macfarlane, 2019).

*Corresponding author. Tel.:+35722893450.
*E-mail address:* stimo@ucy.ac.cy

An alternative direction is to consider macroscopic traffic dynamics based on the concept of the Macroscopic Fundamental Diagram (MFD) (Daganzo, 2007). In this context, an urban area is partitioned into a set of homogeneous regions (Ji and Geroliminis, 2012) within which traffic dynamics are described by the relationships between the three main mobility parameters: speed, flow, and density. MFD modeling considers the free-flow and congested regimes separated at the critical density. In the *free-flow regime*, the flow increases as density increases, up to the critical density. Beyond the critical density, in the *congested regime*, the flow decreases with higher densitie (Daganzo, 2007). Macroscopic modeling reproduces the recurrent dynamics of congestion based on aggregated traffic data (Bellocchi and Geroliminis, 2020) and utilizes an MFD to estimate the *outflow* of a region (Geroliminis and Daganzo, 2008). Therefore, macroscopic modeling enables the development of traffic management solutions that require aggregate data points and fewer parameters to be calibrated (Geroliminis and Sun, 2011).

Traffic congestion mitigation strategies that take advantage of the MFD include perimeter and gating control (Keyvan-Ekbatani et al., 2012; Haddad and Geroliminis, 2012; Saeedmanesh et al., 2021). These strategies aim to ensure that a protected region will always operate in the free-flow regime. This is achieved by regulating the vehicle entries at the boundary of the protected region, e.g., using street closures or traffic light control (Kouvelas et al., 2017). A limitation of perimeter control strategies is that they cannot totally eliminate congestion, but they shift it to the boundary of the protected region (Tsitsokas et al., 2023). Another approach is the macroscopic route guidance strategy that balances the traffic load across regions by imposing to vehicular flows regional-level paths to follow (Hajiahmadi et al., 2013). In this direction, a novel route guidance multi-regional strategy is proposed by Leclercq et al. (2021) where congested regions are avoided from routing instructions. In addition, the effect of route choice on MFD modeling within heterogeneous urban networks is explored in the work of Yildirimoglu et al. (2015). The latter demonstrates that route guidance can avoid hysteresis in MFD models except from high-demand scenarios where there is high inconsistency between the model and the physical plant. Hence, despite the fact that regional route guidance can significantly reduce travel times, it has limited effectiveness when demand is higher than capacity, e.g., during rush hours (Daganzo, 2007).

As an alternative, demand management methodologies (Luten, 2004) manage traffic demand (i.e., number of vehicles requesting to enter the network at a particular time) to avoid traffic congestion before its emergence. In this direction, Menelaou et al. (2019) proposed a route-reservation architecture along with demand management and route guidance to eliminate congestion. In this approach, traffic is redistributed in both time and space by controlling the departure time and routes of drivers, indicating that the integration of demand management with route guidance can significantly benefit the network operation. In a follow-up work by Menelaou et al., 2021b, a joint route guidance and demand management strategy with macroscopic traffic dynamics was proposed. In this scheme, traffic flows are guided to follow regional-level paths (route guidance) and delay departures (demand management) if these actions minimize the total time spent of all vehicles in the network. However, within the macroscopic models even a limited number of shifts in the departure times of travellers can significantly reduce the total travel time spent in the network as shown in the work of Yildirimoglu and Ramezani (2020). Similar findings are also derived in the work of Kumarage et al. (2021) in which a macroscopic demand redistribution[1] strategy is proposed to minimize the total time spent in a two-region urban network.

Regional traffic management strategies can be implemented in a Model Predictive Control (MPC) framework (Maciejowski, 2002). Within the MPC framework, the MFD dynamics can serve as the prediction model, while various strategies can be considered, such as the joint integration of perimeter control with route guidance (Sirmatel and Geroliminis, 2018) and (Menelaou et al., 2021a). An important challenge of the MPC framework is that macroscopic traffic dynamics are often nonlinear, resulting in non-convex mathematical programs (Hajiahmadi et al., 2015). Non-convex MPC problems are hard to be optimally solved, often leading to inadequate quality solutions (Hajiahmadi et al., 2015). To address this issue, Groot et al. (2012) and Menelaou et al. (2019) approximate the nonlinear MPC problem with Mixed Integer Linear Programs (MILPs). Although such approaches can obtain the optimal solution, they are impractical for real-time applications as they are computationally demanding. On that account, Kouvelas et al. (2019); Sirmatel et al. (2021); Sirmatel and Geroliminis (2021), and Genser and Kouvelas (2020) linearize the perimeter control and route guidance problems, respectively, utilizing real-time state estimates to form piecewise linear functions. Although both approaches are fast, no information is provided regarding the quality of the derived

[1]The term, Macroscopic demand redistribution, refers to the action of redistributing traffic demand by taking macroscopic control decisions, which involve adjusting the flow rates of traffic demand over time.

solutions compared to the optimal. Similarly, Menelaou et al. (2020) and Menelaou et al. (2021b) study the joint route guidance and demand management problem with triangular and third order polynomial shaped MFDs, respectively, and develop linear programming formulations that yield almost optimal solutions and tight optimality bounds. A limitation of the latter approaches is that they require a specific (e.g. third-order polynomial) rather than a generalized MFD shape. The term generalized MFD shaped refer to the fact that this works do not necessarily assume that MFD follows a specific MFD shape (e.g., triangular or third order polynomial). This work addresses this limitation by proposing two solution approaches to efficiently solve the regional route guidance and demand management problem that consider generalized MFD shapes.

In particular, this work proposes the development of two different solution approaches for the regional route guidance and demand management with generalized MFD dynamics, extending on our previous work that utilized triangular MFD shapes (Menelaou et al., 2021b). On the one hand, the consideration of triangular MFD shapes implies a linear relationship between flow and density and a constant speed in the free-flow regime leading to linear and easily solvable formulations when imposing free-flow conditions, but limits the accuracy of the actual macroscopic traffic dynamics. On the other hand, the consideration of generalized MFD shapes allows accurate representation of traffic dynamics, but results in several nonlinearities that make the problem challenging to solve. These challenges are addressed in this paper.

Specifically, we develop two different solution approaches for the regional route guidance and demand management problem: (i) a successive convexification approach, and (ii) a linear approximation approach. Both approaches can offer accurate and close to optimal control decisions assuming generalized MFD dynamics in real-time. The successive convexification approach is comprised of four steps. First, we develop an outer approximation procedure to construct convex sets of all nonlinearities using appropriate traffic state bounds. This approximation relaxes the constraints and therefore the obtained solution may be infeasible compared to the original problem. Second, we utilize the constructed sets to formulate and solve a linear program that approximates the original nonconvex problem. The obtained solution, which may be outside the feasible set of the original problem, is then properly manipulated, to yield a feasible solution. Third, we derive future state estimates by running a macroscopic simulation with the actual nonlinear traffic dynamics utilizing the derived feasible solution. Fourth, we tighten the traffic state bounds using the derived state estimates with the procedure repeating from the first step. In this way, the feasible set is tightened in successive iterations until convergence. The linear approximation approach, first approximates in the least-squares sense the generalized MFD with a triangular one and then solves the related problem using the algorithmic procedure proposed by the authors in (Menelaou et al., 2021b) that considered triangular shape MFDs. We highlight that both solution approaches are customizable and can be employed by transportation researchers to develop online solutions for different real-life traffic control problems. Furthermore, the developed approaches offer global optimality bounds, computed by obtaining lower and upper bounds on the global optimum of the considered problem. The results of the proposed solution approaches are shown to be in agreement under both microscopic and macroscopic simulations, offering high travel time reduction and congestion mitigation. Finally, extensive simulation results indicate that both approaches can offer clear advantages in both execution time and solution quality compared to a state-of-practice nonlinear solver. Nonetheless, to the authors' knowledge, this is the first work in the literature that:

- Develops a successive convexification approach that provides fast and high-quality solutions to the problem of regional route guidance and demand management with generalized MFD dynamics and yields global optimality bounds. Global optimality bounds are computed by obtaining lower and upper-bounds on the global optimum of the considered problem. A lower-bound is obtained from the first iteration of the first algorithmic step, as the original feasible set is outer-approximated by a convex set, while upper-bounds are obtained from the second step in each iteration.

- Develops a linear approximation approach that provides very fast and good quality solutions for the problem of regional route guidance and demand management with generalized MFD dynamics.

The remainder of this work is organized as follows. Section 2 presents the multi-regional modeling framework for route guidance and demand management, and mathematically formulates the joint demand and traffic management problem within an MPC framework. Section 3 proposes an approach to obtain lower bounds on the optimal solution and develops the successive convexification and linear approximation solution approaches to the considered problem. Section 4 presents simulation results and compares the derived solutions from the two developed approaches with

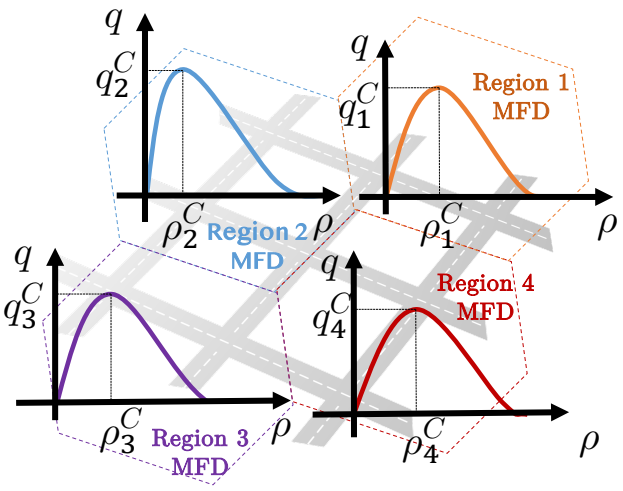


Figure 1: A four region traffic network where the outflow traffic dynamics are modelled with a generalized MFD for each region.

the solution of a state-of-practice nonlinear solver in terms of optimality and execution time. Section 4 also includes extensive microsimulation results demonstrating that the successive convexification approach can substantially reduce the total time spent and avoid the emergence of congestion. Section 5 provides a discussion of the results findings while Section 6 concludes this work and discusses future research directions. Finally, Appendix A develops an outer convexification approach for density and speed MFD functions, Appendix B describes the procedure for the approximation of a generalized with a triangular MFD and Appendix C provides an overview of the notation used in this work.

## 2. Problem Statement

This section provides the multi-regional system model considered in this work and formulates the joint route guidance and demand management problem.

### *2.1. Macroscopic Traffic Flow Model*

In this work we consider an urban traffic network clustered into $|\mathcal{R}|$ homogeneous regions (Ji and Geroliminis, 2012), where $\mathcal{R} = \{1, \ldots, |\mathcal{R}|\}$ represents the set of regions. We assume macroscopic traffic dynamics within each considered region $r \in \mathcal{R}$ which are defined with the use of a generalized MFD shape, as depicted in Fig 1. The time horizon is quantized into time-slots of duration $T_s$, while $L_r$ and $l_r$ denote the total length of region $r \in \mathcal{R}$ and the average trip length of vehicles inside region $r \in \mathcal{R}$, respectively. Moreover let parameters $\rho_r^J$ and $\rho_r^C$ represent the *jam density*, and the *critical density* of region $r$, respectively. Additionally, the variable $q_r(\rho_r(\tau))$ (veh/h) denotes the *intended outflow*[2] of region $r$ at a discrete time-step $\tau$ which is a function of density $\rho_r(\tau)$ (veh/km). According to the macroscopic modeling, $q_r(\rho_r(\tau))$ (veh/h) is equal to the product of variables of density $\rho_r(\tau)$ (veh/km) and speed $v_r(\rho_r(\tau))$ (km/h) such that

$$q_r(\rho_r(\tau)) = \frac{\rho_r(\tau) v_r(\rho_r(\tau)) L_r}{l_r}. \tag{1}$$

The "intended outflow" $q_r(\rho_r(\tau))$ implies the total flow that $r$ can transmit to the outside world (i.e., completed trips) and/or its neighboring regions when the interchanged flows between regions are not restricted from their inter-boundary capacity limitations. It has been empirically observed that $q_r(\rho_r(\tau))$ is well-approximated by an asymmetric

[2]Note that the intended outflow is directly related with the production $P_r(n_r(\tau))$ (veh·km/h) which is a function of the number of vehicles $n_r(\tau)$ that are currently in $r \in \mathcal{R}$ such that $n_r(\tau) = \rho_r(\tau) L_r$. In this way the fundamental relation of traffic can also be expressed as $P_r(n_r(\tau)) = v_r(n_r(\tau)) n_r(\tau)$.

unimodal curve (Geroliminis and Daganzo, 2008) as

$$q_r(\rho_r(\tau)) = \frac{f_r(\rho_r(\tau))L_r}{l_r} \tag{2}$$

where $f_r(\rho_r(\tau))$ is a generalized nonlinear function, termed *generalized MFD*. We consider that the shape of $f_r(\rho_r(\tau))$ has the following properties: (i) it is a continuous and continuously differentiable function, (ii) it is unimodal, increasing in the interval $[0, \rho_r^C]$ and decreasing in the interval $[\rho_r^C, \rho_r^J]$, and (iii) it is concave in the interval $[0, \rho_r^I]$, as well as convex and strictly monotonically decreasing in the interval $[\rho_r^I, \rho_r^J]$, where $\rho_r^I$ is an *inflection point* at which the function changes from concave to convex. According to the fundamental relationship of Eq. (1), the average speed in region $r$ relates to the intended outflow through the relationship

$$v_r(\rho_r(\tau)) = g_r(\rho_r(\tau)) = \frac{f_r(\rho_r(\tau))}{\rho_r(\tau)}. \tag{3}$$

The following properties are assumed for $g_r(\rho_r(\tau))$: (i) it is a continuous and continuously differentiable function, (ii) it is convex and strictly monotonically decreasing, (iii) it is always positive, and (iv) the maximum speed in the region, $v_r^{MAX}$, is attained for zero density, i.e., $v_r^{MAX} = g_r(0)$. Note that, in macroscopic modeling all the variables of speeds and flows are function of the density, i.e., $\rho_r(\tau)$ but for the shake of notational simplicity we drop index $\rho(\tau)$ and is replaced by the index of time $\tau$.

Let $\mathcal{O} \subseteq \mathcal{R}$ and $\mathcal{D} \subseteq \mathcal{R}$ denote the sets of origin and destination regions of different flows, respectively. Also, let $\mathcal{J}_r^- \subseteq \mathcal{R}$ denote the set of neighbouring regions directly accessible from region $r \in \mathcal{R}$, and similarly let $\mathcal{J}_r^+ = \mathcal{J}_r^- \cup \{r\}$, such that

$$\mathcal{J}_r = \begin{cases} \mathcal{J}_r^+, \text{ if } r \in \mathcal{D}, \\ \mathcal{J}_r^-, \text{ otherwise.} \end{cases} \tag{4}$$

Furthermore, let variable $d_{od}(\tau)$ (veh) denote the *instantaneous external demand* which determines the number of vehicles that require to start a trip from $o \in \mathcal{O}$ to $d \in \mathcal{D}$ at time-step $\tau$. Likewise the variable $\tilde{d}_{od}(\tau)$ (veh) is the *admitted external demand* that represents the actual number of vehicles that are allowed to start their trip at $\tau$. In other words, the admitted external demand represents the portion of the external demand that is admitted to enter the network by the demand management strategy with the non-admitted demand waiting at the origin. Moreover, the external demand can also be restricted by the ability of a region to accommodate more vehicles based on its current available capacity and the maximum possible demand that can physically enter the region. Let. parameter $D_{od}^{MAX}$ denote the maximum demand that can physically enter region $o \in \mathcal{O}$ such that $\tilde{d}_{od}(\tau) \leq D_{od}^{MAX}$. In this context, let the *cumulative external demand* $D_{od}(\tau)$ (veh) be used to keep track of the demand that remains outside the network at time-step $\tau$ such that

$$D_{od}(\tau + 1) = D_{od}(\tau) - \tilde{d}_{od}(\tau) + d_{od}(\tau), \quad \tau = 1, 2, \ldots, \tag{5}$$

where, $D_{od}(1) = 0$.

Furthermore, to account for the portion of traffic destined to different regions, we introduce variables $\rho_{rd}(\tau)$ which denote the density in region $r \in \mathcal{R}$ towards $d \in \mathcal{D}$. Clearly, the following relationship holds:

$$\rho_r(\tau) = \sum_{d \in \mathcal{D}} \rho_{rd}(\tau). \tag{6}$$

Similarly, variables $q_{rd}(\tau)$ and $q_{rjd}(\tau)$ denote the *intended transfer flow* from $r \in \mathcal{R}$ to $d \in \mathcal{D}$ and from $r \in \mathcal{R}$ to $d \in \mathcal{D}$, through neighbouring region $j \in \mathcal{J}_r$ at time-step $\tau$, respectively, defined as

$$q_{rd}(\tau) = \frac{v_r(\tau)\rho_{rd}(\tau)L_r}{l_r}, \tag{7}$$

$$q_{rd}(\tau) = \sum_{j \in \mathcal{J}_r} q_{rjd}(\tau), \tag{8}$$

$$q_r(\tau) = \sum_{d \in \mathcal{D}} q_{rd}(\tau), \tag{9}$$

$$q_r(\tau) = \sum_{d \in \mathcal{D}} \sum_{j \in \mathcal{J}_r} q_{rjd}(\tau), \tag{10}$$

Note that the flow of vehicles that arrive at their destination $d \in \mathcal{D}$ and exit the network at time-step $\tau$ is determined by $q_{ddd}(\tau)$, i.e. variable $q_{rjd}(\tau)$ when $\{r = j = d\}$.

The flow that can be exchanged between region $r \in \mathcal{R}$ and its neighbours is limited by the flow/storage capacity of its neighbouring regions $j \in \mathcal{J}_r^-$ with variable $C_{rj}(\rho_j(\tau))$, denoting the inter-boundary capacity from region $r$ to region $j$. The inter-boundary capacity specifies the maximum flow that can be exchanged between the two neighbouring regions and it is a function of the density of the neighbouring region $j$. According to Yildirimoglu et al. (2018), $C_{rj}(\rho_j(\tau))$ can be modelled as

$$C_{rj}(\rho_j(\tau)) = \begin{cases} C_{rj}^{\text{MAX}}, & \text{if } \rho_j(\tau) \leq \beta_{rj}\rho_j^J, \\ \frac{C_{rj}^{\text{MAX}}}{1-\beta_{rj}}\left(1 - \frac{\rho_j(\tau)}{\rho_j^J}\right), & \text{otherwise,} \end{cases} \tag{11}$$

where $C_{rj}^{\text{MAX}}$ is the maximum inter-boundary capacity and $\beta_{rj}\rho_j^J$ is the point where the inter-boundary capacity starts to decrease with $0 < \beta_{rj} < 1$. Therefore, the intended transfer flow is limited by the density in region $r \in \mathcal{R}$, while the transfer flow of the neighbouring region $j$ is analogous to its remaining storage capacity and also depends on the transfer flows from other regions $s \in \mathcal{J}_r^-$. Hence, the *actual transfer flow* from $r \in \mathcal{R}$ to $j \in \mathcal{J}_r$, denoted by variable $\tilde{q}_{rjd}(\tau)$, is defined as

$$\tilde{q}_{rjd}(\tau) = \min\left(q_{rjd}(\tau), C_{rj}(\rho_j(\tau))\frac{q_{rjd}(\tau)}{\sum_{y \in D} q_{rjy}(\tau)}\right). \tag{12}$$

Taking the above into account, the traffic dynamics of density of region $r \in \mathcal{R}$ towards region $d \in \mathcal{D}$ is expressed as

$$\rho_{rd}(\tau + 1) = \rho_{rd}(\tau) + \frac{1}{L_r}\tilde{d}_{rd}(\tau) + \frac{T_s}{L_r}\left(\sum_{j \in \mathcal{J}_r^-} \tilde{q}_{jrd}(\tau) - \sum_{j \in \mathcal{J}_r} \tilde{q}_{rjd}(\tau)\right). \tag{13}$$

### *2.2. Problem Formulation*

The objective of the considered problem is to minimize the *Total Time Spent* (TTS) of all vehicles, which is the sum of the *Total Travel Time* (TTT) and the *Total Waiting Time* (TWT) of all vehicles in the network. Note that TWT is the cumulative time that vehicles may be imposed to wait outside the network, calculated as the difference between the time that they request to start their trip and the time that they are admitted in the network.

#### *2.2.1. Objective function*

To define the objective function we introduce variables $S^a(\tau)$ that represent the cumulative number of vehicles that request to enter the road network and $S^b(\tau)$ that denote the cumulative number of vehicles successfully arriving at their destination at time-step $\tau$, mathematically defined as

$$S^a(\tau + 1) = S^a(\tau) + \sum_{o \in \mathcal{O}}\sum_{d \in \mathcal{D}} d_{od}(\tau), \ \tau = 1, 2, \ldots, \tag{14}$$

$$S^b(\tau + 1) = S^b(\tau) + T_s \sum_{d \in \mathcal{D}} q_{ddd}(\tau), \ \tau = 1, 2, \ldots, \tag{15}$$

where $S^a(1) = 0$ and $S^b(1) = 0$. Then the objective function, is defined as the summation of the difference between $S^a(\tau)$ and $S^b(\tau)$ over all time-steps. Hence the objective function denotes the Total Time Spent (TTS) of all vehicles in the network, $J_{TTS}$ (veh·h), defined as

$$J_{TTS} = T_s \sum_{\tau}(S^a(\tau) - S^b(\tau)). \tag{16}$$

Note that TTS is the sum of TWT and TTT (i.e., TTS=TTT+TWT).

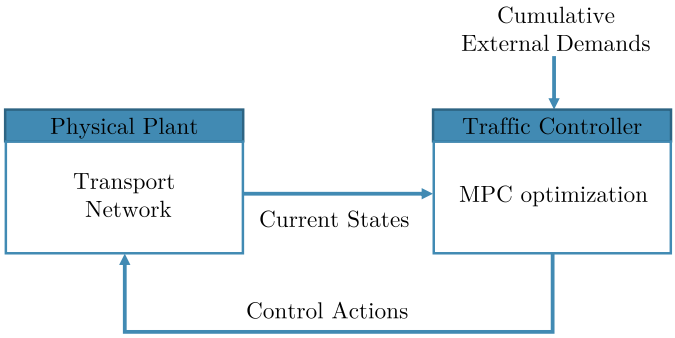


Figure 2: Block diagram describing the general operation of the proposed MPC scheme.

*2.2.2. General Model Predictive Control Framework*

The block diagram in Fig. 2 describes the general Model Predictive Control (MPC) framework used in this work. The framework has time-steps of duration $T_s$, such that a different control action is applied at every time-step. Each MPC problem considers a control and prediction horizon of duration $N^P$ time-steps, while a new MPC problem is solved every $N^C \leq N^P$ time-steps. At time-step $t = N^C(p-1)$, the measured current states $\bar{\rho}_r(t)$, $\bar{\rho}_{rd}(t)$ of the physical plant and the cumulative external demands $\bar{D}_{rd}(t)$ are used as input to the traffic controller to solve the $p$th MPC optimization problem, for the time horizon $\mathcal{T}_p = \{N^C(p-1)+1, \ldots, N^C(p-1)+N^P\}$. The main control decisions used in the MPC problem are the intended transfer flows interchanged between neighboring regions, $q_{rjd}(\tau)$ (route guidance), and the admitted external flows $\tilde{d}_{od}(\tau)$ (demand management). Upon solution of an MPC problem, the derived decisions are used as the control input to the physical plant with the procedure repeated every $N^C$ time-steps. The $p$th MPC problem can be formulated as the following mathematical program:

$$(\mathrm{P}_1) \quad \text{Minimize } T_s \sum_{\tau \in \mathcal{T}_p} (S^a(\tau) - S^b(\tau)) \tag{17a}$$

Subject to: Traffic dynamics: (2) – (15),

$$\tilde{d}_{od}(\tau) \leq D_{od}^{MAX}, \ \forall \tau \in \mathcal{T}_p, \forall o \in \mathcal{O}, \forall d \in \mathcal{D}, \tag{17b}$$

$$\tilde{d}_{od}(\tau) \leq D_{od}(\tau), \ \forall \tau \in \mathcal{T}_p, \forall o \in \mathcal{O}, \forall d \in \mathcal{D}, \tag{17c}$$

$$0 \leq \rho_r(\tau) \leq \rho_r^J, \forall \tau \in \mathcal{T}_p, \forall r \in \mathcal{R}, \tag{17d}$$

$$\text{Initialization: } \rho_r(t) = \bar{\rho}_r(t), \ \forall r \in \mathcal{R}, \ \rho_{rd}(t) = \bar{\rho}_{rd}(t), \ D_{rd}(t) = \bar{D}_{rd}(t), \forall r \in \mathcal{R}, \forall d \in \mathcal{D}, \ t = N^C(p-1), \tag{17e}$$

$$\text{Variables: } S^a(\tau), \ S^b(\tau), \ \forall \tau \in \mathcal{T}_p, \ \rho_r(\tau), \ q_r(\tau), \ v_r(\tau), \ \forall r \in \mathcal{R}, \forall \tau \in \mathcal{T}_p, \ \rho_{rd}(\tau), \ \tilde{d}_{od}(\tau), \ D_{rd}(\tau), \ q_{rd}(\tau),$$
$$\forall r \in \mathcal{R}, \forall o \in \mathcal{O}, \ \forall d \in \mathcal{D}, \forall \tau \in \mathcal{T}_p, \ q_{rjd}(\tau), \ \tilde{q}_{rjd}(\tau), \ \forall r \in \mathcal{R}, \ \forall j \in \mathcal{J}, \ \forall d \in \mathcal{D}, \forall \tau \in \mathcal{T}_p.$$

In Problem $\mathrm{P}_1$, constraints (2) - (15) model the traffic dynamics according to a generalized MFD, (17b) and (17c) impose the physical limits on the external demand inflows ensuring that it is always smaller than the maximum possible external inflow $D_{od}^{MAX}$ and the total external demand $D_{od}(\tau)$, (17d) makes sure that the density of each region is between the physical limits, and (17e) represent the initial state of the network. Problem $(P_1)$ is a non-convex nonlinear Program (NLP) due to existence of the nonlinear unimodal MFD function in (2), the decreasing speed function in (3), the bilinear term in (7), and the nonlinear functions in (11) and (12).

By solving Problem $\mathrm{P}_1$, the control actions $q_{rjd}(\tau)$ and admitted external flows $\tilde{d}_{od}(\tau)$, for $\tau \in \{N^C(p-1)+1, \ldots, N^C(p-1)+N^C\}$ are applied to the *physical plant*, i.e. the real-life traffic network. Nonetheless, the solution of $\mathrm{P}_1$ may lead to a different solution of the physical plant due to modeling uncertainties or noisy measurements. To reduce their effect, we consider the split ratios rather than the intended transfer flows for route guidance because the former are relative quantities. Specifically, *split ratios*, $\gamma_{rjd}(\tau) \in [0,1]$ are expressed as

$$\gamma_{rjd}(\tau) = \begin{cases} q^*_{rjd}(\tau)/q^*_{rd}(\tau), & \text{for } q^*_{rd}(\tau) \neq 0, \\ 1/|\mathcal{J}_r|, & \text{for } q^*_{rd}(\tau) = 0, \end{cases} \quad r \in \mathcal{R}, \ j \in \mathcal{J}_r, \ d \in \mathcal{D}, \ \tau \in \mathcal{T}_p. \tag{18}$$

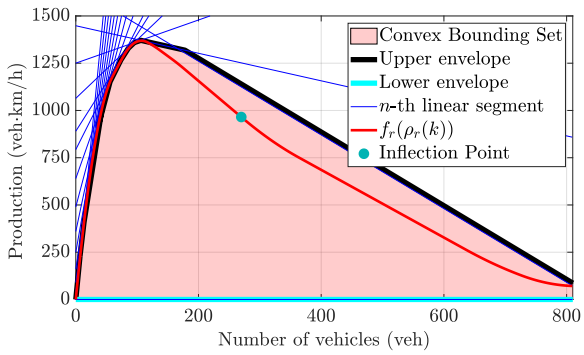


Figure 3: Example of the bounding set constraints comprised of piecewise linear segments used to derive an outer approximation to the flow MFD relationship given by Eq. (2).

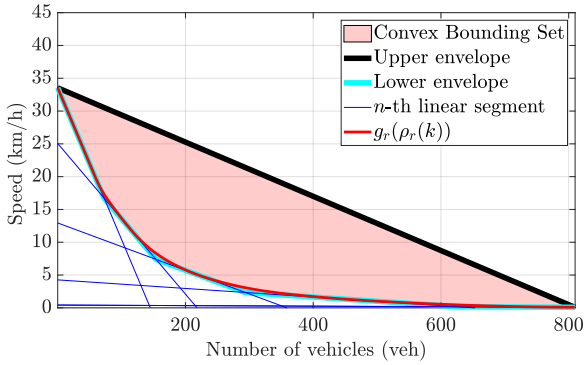


Figure 4: Example of the bounding set constraints comprised of piecewise linear segments used to derive an outer approximation to the speed MFD relationship given by Eq. (3).

where $q^*_{rjd}(\tau)$ and $q^*_{rd}(\tau)$ denote the obtained flows from the solution of the optimization problem. Hence, in the physical plant we assume that $q^*_{rjd}(\tau) = \gamma_{rjd}(\tau) q^*_{rd}(\tau)$, in such a way that $\sum_{j \in \mathcal{J}_r} \gamma_{rjd}(\tau) = 1$, $r \in \mathcal{R}$, $d \in \mathcal{D}$. Notice in Eq. (18) that when $q^*_{rd}(\tau) = 0$ any appearing flows in the physical plant are equally split among neighbouring regions.

The following Section 3 presents the two convex solution approaches of the considered MPC problem that build upon the requirements/properties of the proposed generalized MFD shape.

## 3. Proposed Solutions

In this section, we first relax Problem $\mathrm{P}_1$ to obtain a lower-bound solution (Section 3.1). Optimality is achieved when the obtained lower-bound solution is feasible. Otherwise, the solution can be used as a starting point to achieve high-quality feasible solutions (upper-bounds). Towards this direction, we propose the *Successive Convexification Route Guidance and Demand Management* (SC-RGDM) algorithm. An alternative solution is the *Linear Approximation Route Guidance and Demand Management* (LA-RGDM) that approximates Problem ($\mathrm{P}_1$) with a linear program upon approximation of generalized with triangular MFDs.

### *3.1. Lower-bound Solution to Problem $P_1$*

In this section we proposed a linear relaxation of Problem ($\mathrm{P}_1$) by relaxing all nonconvex constraints with convex outer approximation constraints. The proposed relaxation results in a Linear Program which provides a lower-bound solution to the objective function of the original problem ($\mathrm{P}_1$) that can be used to derive an optimality gap of any developed solution methodology. Next, we approximate the five non-convex constraints of Problem ($\mathrm{P}_1$), namely, (2), (3), (7), (11) and (12) with convex bounding sets.

First, Eq. (2) is convexified by constructing a convex *outer approximation* of the generalized flow-density MFD under density box constraints using piecewise linear segments. In this way, we define the convex bounding set $\mathcal{S}^q_{r\tau}$, $r \in \mathcal{R}$, $\forall\ \tau$, such that $(q_r(\tau), \rho_r(\tau)) \in \mathcal{S}^q_{r\tau}$. Set $\mathcal{S}^q_{r\tau}$ is defined as

$$\begin{aligned} \mathcal{S}^q_{r\tau} = \Big\{ & (q_r(\tau), \rho_r(\tau)) \in \mathbb{R}^2 \,|\, \rho^l_r(\tau) \leq \rho_r(\tau) \leq \rho^u_r(\tau) \text{ and} \\ & q_r(\tau) \leq \widehat{a}_{r\tau n} \rho_r(\tau) + \widehat{b}_{r\tau n}, n \in \widehat{\mathcal{N}}^q_{r\tau},\ q_r(\tau) \geq \breve{a}_{r\tau n} \rho_r(\tau) + \breve{b}_{r\tau n},\ n \in \breve{\mathcal{N}}^q_{r\tau} \Big\}, \end{aligned} \tag{19}$$

where, the parameter $\rho^l_r(\tau)$ denotes the upper and $\rho^u_r(\tau)$ the lower-bound of density. Moreover, $\breve{\mathcal{N}}^q_{r\tau}$ and $\widehat{\mathcal{N}}^q_{r\tau}$ denote the sets of piecewise linear segments comprising the lower and upper envelopes that approximate $q_r(\tau) = f_r(\rho_r(\tau))$ from below and above respectively, as shown in Fig. 3. The outer approximation procedure to derive parameters $\widehat{a}_{r\tau n}$, $\widehat{b}_{r\tau n}$, $\breve{a}_{r\tau n}$ and $\breve{b}_{r\tau n}$ is described in Appendix A.

In a similar fashion, we convexify Eq. (3) by constructing convex bounding polyhedral sets $\mathcal{S}^v_{r\tau}$, $r \in \mathcal{R}$, $\forall \tau \in \mathcal{T}_p$, such that $(v_r(\tau), \rho_r(\tau)) \in \mathcal{S}^v_{r\tau}$. Set $\mathcal{S}^v_{r\tau}$ is defined as

$$S^v_{r\tau} = \Big\{(v_r(\tau), \rho_r(\tau)) \in \mathbb{R}^2 \,|\, \rho^l_r(\tau) \le \rho_r(\tau) \le \rho^u_r(\tau) \text{ and } v_r(\tau) \le \widehat{c}_{r\tau n}\rho_r(\tau) + \widehat{d}_{r\tau n},\ n \in \widehat{\mathcal{N}}^v_{r\tau},\ v_r(\tau) \ge \breve{c}_{r\tau n}\rho_r(\tau) + \breve{d}_{r\tau n},\ n \in \breve{\mathcal{N}}^v_{r\tau}\Big\}, \tag{20}$$

where $\breve{\mathcal{N}}^v_{r\tau}$ and $\widehat{\mathcal{N}}^v_{r\tau}$ denote the sets of piecewise linear segments comprising the lower and upper envelopes that approximate $v_r(\tau) = g_r(\rho_r(\tau))$ from below and above respectively, as shown in Fig. 4. The procedure to derive parameters $\widehat{c}_{r\tau n}$, $\widehat{d}_{r\tau n}$, $\breve{c}_{r\tau n}$ and $\breve{d}_{r\tau n}$ is also described in Appendix A.

To convexify the bilinear term of Eq. (7), i.e., $\rho_{rd}(\tau)v_r(\tau)$, the McCormick envelope method is used, (McCormick, 1976). According to McCormick, the product of two box-constrained variables $z = xy$ with $x^l \le x \le x^u$ and $y^l \le y \le y^u$, can be convexified through the construction of the following four half-spaces using the lower and upper-bounds of the two variables:

$$z \ge x^l y + x y^l - x^l y^l, \tag{21}$$

$$z \ge x^u y + x y^u - x^u y^u, \tag{22}$$

$$z \le x^u y + x y^l - x^u y^l, \tag{23}$$

$$z \le x y^u + x^l y - x^l y^u. \tag{24}$$

Constraints (21) - (22) and (23) - (24) are referred to as *underestimator* and *overestimator* half-spaces because they lie below and above the surface $z = xy$, respectively. Assuming that $\rho^l_{rd}(\tau) \le \rho_{rd}(\tau) \le \rho^u_{rd}(\tau)$ and $v^l_r(\tau) \le v_r(\tau) \le v^u_r(\tau)$, Eqs. (21) - (24) can be applied through the mapping $x \equiv \rho_{rd}(\tau)$, $y \equiv v_r(\tau)$ and $z \equiv q_{rd}(\tau)$.

The constraints (11) and (12) are handled together similar to our previous work (Menelaou et al., 2021b). Since constraint (12) is the minimum of two functions, it can be convexified by replacing the equality "=" with the inequality sign "≤" as follows,

$$\tilde{q}_{rjd}(\tau) \le q_{rjd}(\tau), \tag{25}$$

$$\tilde{q}_{rjd}(\tau) \le C_{rj}(\rho_j(\tau)) \frac{q_{rjd}(\tau)}{\sum_{y \in \mathcal{D}} q_{rjy}(\tau)}. \tag{26}$$

Next, as (26) is still non-convex, we further relax constraint (26) by taking the sum over all $\tilde{q}_{rjd}(\tau)$ for $d \in \mathcal{D}$ as follows,

$$\sum_{d \in \mathcal{D}} \tilde{q}_{rjd}(\tau) \le C_{rj}(\rho_j(\tau)), \tag{27}$$

which is a relaxed version of (26). This is due to the fact that individual constraints are always at least as tight as the sum of the associated constraints. As constraint (27) is still non-convex because $C_{rj}(\rho_j(\tau))$ is nonlinear, by combining (25) and (26), constraint (27) can be further reduced into

$$\sum_{d \in \mathcal{D}} \tilde{q}_{rjd}(\tau) \le C^{MAX}_{rj}, \tag{28}$$

$$\sum_{d \in \mathcal{D}} \tilde{q}_{rjd}(\tau) \le \frac{C^{\text{MAX}}_{rj}}{1 - \beta_{rj}} \Big(1 - \frac{\rho_j(\tau)}{\rho^J_j}\Big), \tag{29}$$

for all $\tau \in \mathcal{T}_l$, $r \in \mathcal{R}$, $j \in \mathcal{J}_r$. Hence, the nonlinear constraints of (11) and (12) are relaxed into the linear constraints (25), (28) and (29).

Combining all the above approximations we have

$$(\text{P}_2) \quad \text{Minimize } T_s \sum_{\tau \in \mathcal{T}_l} (S^a(\tau) - S^b(\tau)) \tag{30}$$

Subject to: Constraints: (1), (4) – (6), (10), (13) – (15), (17e), (19) – (24), (25), (28) – (29).

Variables: $S^a(\tau)$, $S^b(\tau)$, $\forall \tau \in \mathcal{T}_p$, $\rho_r(\tau)$, $q_r(\tau)$, $v_r(\tau)$, $\forall r \in \mathcal{R}, \forall \tau \in \mathcal{T}_p$, $\rho_{rd}(\tau)$, $\tilde{d}_{od}(\tau)$, $D_{rd}(\tau)$, $q_{rd}(\tau)$, $\forall r \in \mathcal{R}$, $\forall o \in \mathcal{O}$, $\forall d \in \mathcal{D}, \forall \tau \in \mathcal{T}_p$, $q_{rjd}(\tau)$, $\tilde{q}_{rjd}(\tau)$, $\forall r \in \mathcal{R}$, $\forall j \in \mathcal{J}$, $\forall d \in \mathcal{D}, \forall \tau \in \mathcal{T}_p$.

Formulation (30) is a linear program that offers a lower-bound solution to the original problem. Hence, the proposed relaxed formulation (30) may result in an infeasible solution when the obtained solution violates some of the original Problem ($P_1$) constraints. Nonetheless, the lower-bound solution can be used as a starting point to obtain high quality feasible solutions. Indeed, the proposed SC-RGDM approach described in the next section utilizes the lower-bound solution to produce a high quality feasible solution (i.e., upper-bound).

### *3.2. Successive Convexification Route Guidance and Demand Management (SC-RGDM) Approach*

This section proposed the Successive Convexification algorithm for the regional route guidance and demand management problem, termed SC-RGDM, for obtaining a high-quality upper-bound solution. The SC-RGDM algorithm, outlined in Algorithm 1, is a four-step iterative procedure that yields the immediate $N^C$ decisions used as input to the physical plant, i.e., the split ratios $\gamma_{rjd}(\tau)$ and admitted demands $\tilde{d}_{od}(\tau)$, $r \in \mathcal{R}$, $j \in \mathcal{J}_r$, $d \in \mathcal{D}$, $\tau \in \{N^C(p-1)+1, \ldots, N^C(p-1)+N^C\}$. In each iteration, the algorithm converges to a feasible solution by identifying tighter upper and lower-bounds of density.

At the beginning, the algorithm takes as input optimization-related parameters, the current state of the physical system at time $t = N^C(p-1)$, all the traffic network parameters, and the external demand, before initializing the density bounds to their physical limits by setting $\rho_r^l(\tau) = 0$ and $\rho_r^u(\tau) = \rho_r^J$. Then, the following four-step procedure is executed repeatedly.

The first step uses the current density bounds to construct the convex bounding sets of $\mathcal{S}_{r\tau}^q$ and $\mathcal{S}_{r\tau}^v$, $r \in \mathcal{R}$, $\tau \in \mathcal{T}_p$, according to the outer approximation procedure developed in Appendix A. Note that the mathematical program solved in the first iteration from this step is equivalent to Problem $P_2$, as the outer approximation is performed for the entire feasible set. Hence, the optimal objective value of the particular program serves as a lower-bound to the optimal objective value of Problem $P_1$. The second step, uses the current bounds on density and solves Problem $P_2$; then its solution is utilized to compute the split ratios $\gamma_{rjd}(\tau)$ using Eq. (18). In the third step, a macroscopic traffic simulator, that is based on the traffic dynamics (2) - (7), (11) - (15), takes the derived split ratios and the admitted demands as input to produce state estimates for the densities of each region, i.e., $\hat{\rho}_r(\tau)$, $r \in \mathcal{R}$, $\tau \in \mathcal{T}_p$. Note that the use of split ratios explicitly satisfies all model constraints, guaranteeing the production of feasible solutions. The solution obtained from Problem $P_2$ does not have this property due to the various outer approximations performed to convexify the problem. The fourth step uses the estimations of the state to identify tighter lower and upper-bounds on variable $\rho_r(\tau)$; the updated bounds are used in Steps 1 and 2 of the next iteration. Hereafter, the bounds on variable $\rho_r(\tau)$ during iteration $\lambda$ are calculated as follows

$$\rho_r^l(\tau) = (1 - C_\lambda)\hat{\rho}_r(\tau), \qquad \rho_r^u(\tau) = (1 + C_\lambda)\hat{\rho}_r(\tau), \quad r \in \mathcal{R},\ \tau \in \mathcal{T}_p, \tag{31}$$

respectively. $C_\lambda$ is an iteration-dependent constant given by

$$C_\lambda = C\frac{N^I - (\lambda - 1)}{N^I}, \tag{32}$$

where $C \in (0, 1)$ is a constant and $N^I$ denotes the total number of iterations to be performed by Algorithm 1. Note that $C_\lambda$ decreases with the number of iterations which implies that the density bounds become tighter in successive iterations. At the end of the iterative procedure the immediate $N^C$ decisions derived in the $N^I$th iteration are used as input to the physical plant. The same procedure is followed for the entire time horizon, advancing $N^C$ steps at a time.

### *3.3. Linear Approximation Route Guidance and Demand Management (LA-RGDM) Approach*

This section proposes a Linear Approximation approach for the regional route guidance and demand management problem, termed LA-RGDM, to obtain very fast, good quality solutions to Problem $P_1$. Towards this direction, the generalized MFDs are approximated with triangular MFDs facilitating the relaxation of nonlinear constraints with linear ones, as recently proposed by Menelaou et al. (2021b).

In particular, a generalized outflow MFD $f_r(\rho_r(\tau))$ is approximated by a triangular MFD $f_r^T(\rho_r(\tau))$ consisting of two distinct regimes separated by the critical density $\rho_r^C$. The two linear segments of the free-flow and congested

**Algorithm 1** Successive Convexification - Route Guidance and Demand Management (SC-RGDM)

**Input:** Parameters of the problem: $C$, $N^I$ $N^P$, $N^C$, $p$, $t = N^C(p-1)+1$.
Regional traffic state: $\rho_r(t)$, $r \in \mathcal{R}$, $\rho_{rd}(t)$, $r \in \mathcal{R}$, $d \in \mathcal{D}$, $D_{od}(t)$, $o \in \mathcal{O}$, $d \in \mathcal{D}$.
Traffic related parameters: $f_r(\rho)$, $g_r(\rho)$, $r \in \mathcal{R}$, $C_{rj}^{MAX}$, $\beta_{rj}$, $j \in \mathcal{J}_r$, $r \in \mathcal{R}$.
Demand requesting to be served: $d_{od}(\tau)$, $o \in \mathcal{O}$, $d \in \mathcal{D}$, $\tau \in \mathcal{T}_p = \{t,\ t+1, \cdots, t+N^P\}$.
**Initial States:** $\rho_r^l(\tau) = 0$, $\rho_r^u(\tau) = \rho_r^J$, $r \in \mathcal{R}$, $\tau \in \mathcal{T}_p$.
**for** $\lambda = 1$ to $N^I$ **do**
**1:** Obtain $\mathcal{S}_{r\tau}^q$ and $\mathcal{S}_{r\tau}^v$, $r \in \mathcal{R}$, $\tau \in \mathcal{T}_p$, using the outer approximation procedure in Appendix A.
**2:** Execute Problem $P_2$ and identify the ratios $\gamma_{rjd}(\tau)$, $r \in \mathcal{R}$, $j \in \mathcal{J}_r$, $d \in \mathcal{D}$, $\tau \in \mathcal{T}_p$ according to (18).
**3:** Using the identified split rations split ratios $\gamma_{rjd}(\tau)$ and the traffic dynamics of (2) - (7), (11) - (15), of Section 2.1 perform a simulation to predict future state estimates i.e., $\hat{\rho}_r(\tau)$, $r \in \mathcal{R}$, $\tau \in \mathcal{T}_p$.
**4:** Update bounds on variables $\rho_r(\tau)$ using Eq. (31).
**end for**
**Output:** Derived split ratios $\gamma_{rjd}(\tau)$ and admitted demands $\tilde{d}_{od}(\tau)$, $r \in \mathcal{R}$, $j \in \mathcal{J}_r$, $d \in \mathcal{D}$, $\tau \in \mathcal{T}_p$.

regimes are constructed in the intervals $\rho_r(\tau) \in [0, \rho_r^C]$ and $\rho_r(\tau) \in [\rho_r^C, \infty)$ using the optimal least-squares fit, as described in Appendix B. The fitted triangular function is of the form

$$f_r^T(\rho_r(\tau)) = \begin{cases} \delta_{r1}\rho_r(\tau), & 0 \le \rho_r \le \rho_r^C, \\ \delta_{r2}\rho_r(\tau) + \delta_{r3}, & \rho_r^C < \rho_r \le -\delta_{r3}/\delta_{r2}, \end{cases} \tag{33}$$

where $\delta_{r1}, \delta_{r2}$ and $\delta_{r3}$ are fitted parameters with $\delta_{r1}$ and $\delta_{r2}$ denoting the approximated *free-flow* and *backward congestion propagation* speed when considering triangular MFD, respectively.

Although the triangular MFD is comprised of two linear segments, it still results in nonlinearities with respect to constraints (33) and (7). Constraint (33) is relaxed by replacing the equality "=" with the inequality sign"≤" yielding

$$q_r(\tau) \le \delta_{r1}\rho(\tau), \tag{34}$$
$$q_r(\tau) \le \delta_{r2}\rho(\tau) + \delta_{r3}. \tag{35}$$

Furthermore, constraint (7) is relaxed into

$$q_{rd}(\tau) \le \delta_{r1}\rho_{rd}(\tau), \tag{36}$$

since for the triangular MFD it is true that $v_r(\tau) \le v_r^f$ for all densities. Finally, constraints (11) and (12) are jointly handled as in the SC-RGDM approach. Combining the above, yields the following mathematical program that approximates Problem $P_1$.

$$(P_3)\ \text{Minimize}\ \ T_s \sum_{\tau \in \mathcal{T}_l} (S^a(\tau) - S^b(\tau)) \tag{37}$$

Subject to: Constraints: (1), (4) – (6), (10), (13) – (15), (17e), (34) – (36), (25), (28) – (29).

Variables: $S^a(\tau)$, $S^b(\tau)$, $\forall \tau \in \mathcal{T}_p$, $\rho_r(\tau)$, $q_r(\tau)$, $v_r(\tau)$, $\forall r \in \mathcal{R}, \forall \tau \in \mathcal{T}_p$, $\rho_{rd}(\tau)$, $\tilde{d}_{od}(\tau)$, $D_{rd}(\tau)$, $q_{rd}(\tau)$, $\forall r \in \mathcal{R}$, $\forall o \in \mathcal{O}$, $\forall d \in \mathcal{D}, \forall \tau \in \mathcal{T}_p$, $q_{rjd}(\tau)$, $\tilde{q}_{rjd}(\tau)$, $\forall r \in \mathcal{R}\ \forall j \in \mathcal{J}\ \forall d \in \mathcal{D}, \forall \tau \in \mathcal{T}_p$.

Formulation (37) is a Linear Program (LP) that provides an approximate solution to the original Problem $P_1$ which provides neither a lower bound nor a feasible solution to Problem $P_1$. Nonetheless, exploiting the solution of $P_3$ to derive split ratios using Eq. (18) yields good quality feasible solutions, as outlined in Algorithm 2.

## 4. Simulation Results

The proposed approaches are evaluated using both macroscopic and microscopic simulations. At a macroscopic level, a 16-region synthetic network comprised of well-defined third-order polynomial MFDs is considered to evaluate

**Algorithm 2** Linear Approximation - Route Guidance and Demand Management (LA-RGDM)

**Input:** Optimization-related parameters: $N^C$, $p$, $t = N^C(p-1)+1$.
Current state: $\rho_r(t)$, $r \in \mathcal{R}$, $\rho_{rd}(t)$, $r \in \mathcal{R}$, $d \in \mathcal{D}$, $D_{od}(t)$, $o \in \mathcal{O}$, $d \in \mathcal{D}$.
Traffic network parameters: $f_r(\rho)$, $r \in \mathcal{R}$, $C_{rj}^{MAX}$, $\beta_{rj}$, $j \in \mathcal{J}_r$, $r \in \mathcal{R}$.
External demand: $d_{od}(\tau)$, $o \in \mathcal{O}$, $d \in \mathcal{D}$, $\tau \in \mathcal{T}_p = \{t,\ t+1, \cdots, t+N^P\}$.
**1:** Derive an approximate triangular MFD $f_r^T(\rho_r)$, $r \in \mathcal{R}$, using the approximation procedure in Appendix B.
**2:** Solve (37).
**3:** Derive split ratios $\gamma_{rjd}(\tau)$, $r \in \mathcal{R}$, $j \in \mathcal{J}_r$, $d \in \mathcal{D}$, $\tau \in \mathcal{T}_p$ using (18).
**Output:** Split ratios $\gamma_{rjd}(\tau)$ and admitted demands $\tilde{d}_{od}(\tau)$, $\forall\ r \in \mathcal{R}$, $j \in \mathcal{J}_r$, $d \in \mathcal{D}$, $\tau \in \mathcal{T}_p$.

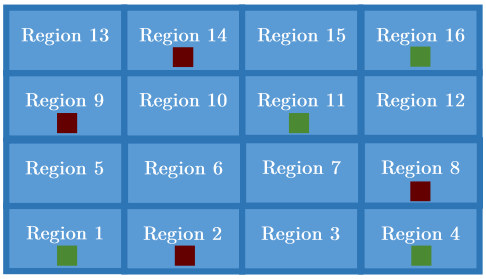


Figure 5: A simulated urban area consisting of 16 regions.

and compare the solution quality and computational efficiency of SC-RGDM and LA-RGDM under no uncertainty. At a microscopic level, a realistic 3-region network is considered within the Simulator for Urban MObility (SUMO Behrisch et al., 2011) to evaluate the effectiveness of SC-RGDM under model uncertainty emanating from the stochastic nature of traffic mobility.

### *4.1. Macroscopic simulation*

#### *4.1.1. Setup*

For the evaluation of the proposed methodology the 16-region synthetic network topology shown in Fig. 5 is considered. Flows are generated randomly from regions 1, 4, 11 and 16 (markers with green colored squares ■) with a random destination selected among regions 2, 8, 9 and 14 (markers with red colored squares ■). The network consists of 16 regions with MFDs of the form $q_r(\tau) = a_{r1}\rho_r^3(\tau)+a_{r2}\rho_r^2(\tau)+a_{r3}\rho_r(\tau)$, with parameter values: $a_{r1} = 8/3675$, $a_{r2} = -1192/2205$, $a_{r3} = 14768/441$, $\rho_r^C = 43$ veh/km, $\rho_r^J = 118$ veh/km, $L_r = 1$ km, $l_r = 0.3$ and $q_r^C = 1850/3$ veh/h, $\forall r \in \mathcal{R}$, $C_{rj}^{\text{MAX}} = 2000$ veh/h, $\beta_{rj} = 0.25$, $\forall r \in \mathcal{R}$, $\forall j \in \mathcal{J}_r$. The MPC parameters are set equal to $T_s = 30$ s, $N^C = 1$ and $N^P = 30$, respectively.

Three traffic scenarios are considered for evaluation purposes: (i) *light* with average demand around 2000 veh/h, (ii) *moderate* with average demand around 3000 veh/h, and (iii) *heavy* with average demand around 4000 veh/h. The demand loading procedure holds for an hour and varies across the O-D pairs. It is also assumed that the compliance rate of drivers is equal to 100% which means that all drivers follow the control inputs of the traffic controller.

In this setting the performance of the following solution approaches is examined:

- **SP** denotes the traffic control strategy where all vehicles follow the shortest travel-time path from their origin to their destination.
- **NLP-RGDM** denotes the solution of Problem $P_1$ obtained from the state-of-practice nonlinear programming solver IPOPT (Biegler and Zavala, 2009).
- **LA-RGDM** denotes the procedure outlined in Algorithm 2. The parameters of the approximated triangular MFD (33) are derived using the fitting procedure described in Appendix B yielding $\delta_{r1} = 4243/297$, $\delta_{r2} = -4257/519$ and $\delta_{r3} = 55091/57$.

| | | Demand Level | | |
|---|---|---|---|---|
| | | Light | Moderate | Heavy |
| ATS (min) | SP | 2.89 | 3.50 | 19.40 |
| | NLP-RGDM | 4.55 | 5.31 | 7.24 |
| | LA-RGDM | 2.82 | 3.34 | 3.77 |
| | SC-RGDM | 2.75 | 3.17 | 3.55 |
| ATT (min) | SP | 2.89 | 3.50 | 6.63 |
| | NLP-RGDM | 2.97 | 3.04 | 2.83 |
| | LA-RGDM | 2.82 | 3.31 | 3.58 |
| | SC-RGDM | 2.75 | 3.14 | 3.33 |
| AWT (min) | SP | 0.0 | 0.00 | 12.74 |
| | NLP-RGDM | 1.58 | 2.25 | 4.41 |
| | LA-RGDM | 0.0 | 0.02 | 0.18 |
| | SC-RGDM | 0.0 | 0.03 | 0.22 |

Table 1: Performance evaluation of different traffic control strategies for varying demand levels.

- **SC-RGDM** denotes the procedure outlined in Algorithm 1 with parameter values $N^I = 10$ and $C = 0.8$ in all considered scenarios.

Note that the optimization problems associated with LA-RGDM and SC-RGDM are solved using the Gurobi mathematical programming solver (Gurobi Optimization Inc., 2016).

*4.1.2. Results*

Table 4.1.2 presents the results of all considered approaches in terms of the Average Time Spent (ATS), Average Travel Time (ATT), and Average Waiting Time (AWT) at the origin. As can be seen from the table, the SP approach leads to increased travel times, especially for high-demand scenarios. Particularly, all the Route Guidance and Demand Management approaches can achieve ATT savings due to their ability to delay vehicles at their origin before starting their journeys. Comparing the three route guidance and demand management approaches, it is clear that the SC-RGDM outperforms the two other approaches as it serves all vehicles with the shortest ATS. In contrast, both SC-RGDM and LA-RGDM yield excellent performance for all considered scenarios, with SC-RGDM having slightly reduced travel times compared with LA-RGDM. Nevertheless, NLP-RGDM yields reduced travel times but with higher waiting times compared to SP, such that the ATS of NLP-RGDM is better than SP only for the heavy demand scenario. Hence, even though NLP-RGDM can lead to shorter ATT, in some instances it may yield higher ATS, imposing unnecessary delays at the origins. Finally, note that although waiting at the origin is not explicitly imposed in the SP scheme, waiting occurs implicitly for vehicles that want to enter during highly congested conditions.

Fig. 6 illustrates the space-time density diagrams of all approaches considering (a) light and (b) heavy load demand scenarios. Fig. 6 (a) indicates that in the light demand scenario all approaches face no severe traffic jam, with LA-RGDM and SC-RGDM having a slightly better performance. On the other hand, Fig. 6 (b) shows that in congested conditions demand management ensures that density is kept around the critical values with all route guidance and demand management approaches achieving travel time savings. In this way, all route guidance and demand management approaches serve vehicles almost two times faster than the SP scheme.

Fig. 7 illustrates the cumulative number of vehicles that request to enter the network (generated) or complete their trips (i.e., exit the network) as a function of time considering the (a) light and (b) heavy load demand scenarios. As can be seen in the figure, all approaches manage to serve all vehicles within the considered simulation time. More specifically, all approaches behave equally well in the light demand scenario, but this is not the case for the heavy demand scenario. Specifically, both figures show that the SC-RGDM approach outperforms the rest of the route guidance and demand management approaches, with the NLP-RGDM having the worse performance in both considered demand scenarios. Therefore, it is evident that the proposed SC-RGDM and LA-RGDM offer significant

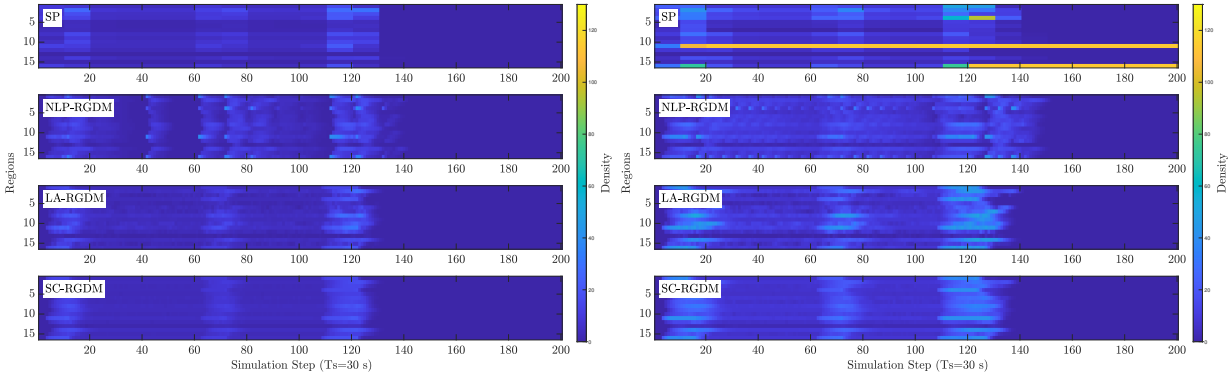


(a) (b)

Figure 6: Space-time density diagrams for the (a) light and (b) heavy demand scenarios.

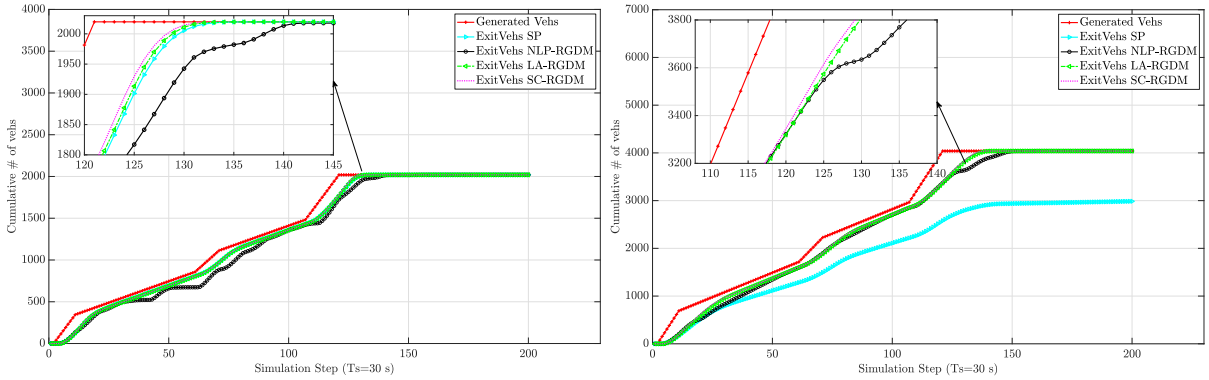


(a) (b)

Figure 7: The cumulative number of vehicles that request to enter the network (Generated vehicles) or complete their trips (i.e., exit vehicles) as a function of time considering the (a) light and (b) heavy load demand scenarios.

| **Scenario** | **Average** | **Execution Time** | | | |
|---|---|---|---|---|---|
| **Number** | **Demand** | NLP-RGDM | LA-RGDM | SC-RGDM | SC & NLP-RGDM |
| 1 | 2000 veh/h | 8.9 s | 1.2 s | 6.9 s | 27 s |
| 2 | 2500 veh/h | 25.3 s | 1.2 s | 6.5 s | 28 s |
| 3 | 3250 veh/h | 30.8 s | 1.2 s | 6.9 s | 30 s |
| 4 | 4000 veh/h | 59.2 s | 1.0 s | 7.0 s | 31 s |
| 5 | 5000 veh/h | 95.6 s | 0.9 s | 7.1 s | 73 s |

Table 2: Execution Time of NLP-RGDM, LA-RGDM and SC-RGDM for varying demand.

reductions in total travel time with enhanced network performance as vehicles manage to reach their destination earlier.

**Algorithm Evaluation.** The quality of the solutions obtained for the three considered route guidance and demand management approaches is compared in terms of execution time and optimality gap. We also introduce the SC & NLP-RGDM approach that denotes the solution of Problem $P_1$ obtained by supplying the final solution of the SC-RGDM

| Scenario Number | Average Demand | Optimality Gap | | | |
|---|---|---|---|---|---|
| | | NLP-RGDM | LA-RGDM | SC-RGDM | SC & NLP-RGDM |
| 1 | 2000 veh/h | 3.8% | 3.4% | 1.1% | 0.9 % |
| 2 | 2500 veh/h | 6.0% | 5.0% | 1.7% | 1.7% |
| 3 | 3250 veh/h | 8.7% | 7.7% | 2.8% | 2.94% |
| 4 | 4000 veh/h | 25.0% | 8.5% | 2.9% | 2.68 % |
| 5 | 5000 veh/h | 10.9% | 9.8% | 2.6% | 2.5% |

Table 3: Optimality Gap of NLP-RGDM, LA-RGDM and SC-RGDM for varying demand.

| Scenario Number | $N^P$ | Demand = 4000 veh/h | | | Demand = 5000 veh/h | | |
|---|---|---|---|---|---|---|---|
| | | NLP-RGDM | LA-RGDM | SC-RGDM | NLP-RGDM | LA-RGDM | SC-RGDM |
| 1 | 5 | 26 s | 0.1 s | 1.7 s | 30 s | 0.1 s | 2.0 s |
| 2 | 10 | 27 s | 0.2 s | 3.0 s | 32 s | 0.2 s | 4.3 s |
| 3 | 15 | 59 s | 0.2 s | 4.8 s | 95 s | 0.2 s | 4.8 s |
| 4 | 20 | 540 s | 0.3 s | 6.5 s | 669 s | 0.3 s | 5.9 s |
| 5 | 30 | 584 s | 0.5 s | 6.8 s | 640 s | 0.5 s | 7.1 s |

Table 4: Average execution time for the solution of one MPC problem using NLP-RGDM, LA-RGDM and SC-RGDM for varying prediction horizon size $N^P = \{5, 10, 15, 20, 30\}$.

approach as the initial point of the nonlinear MPC solver. In particular the *execution time* is defined as the average running time of a particular algorithm for the solution of one MPC problem, while the *optimality gap* is defined as

$$\text{Optimality Gap} = \frac{J_{\text{TTS}}^{\text{Alg}} - J_{\text{TTS}}^{\text{LB}}}{J_{\text{TTS}}^{\text{LB}}} \times 100\%,$$

where $J_{\text{TTS}}^{\text{LB}}$ denotes the lower-bound objective value obtained from the solution of Problem $\text{P}_2$ for the entire time horizon, i.e., $\mathcal{T} = \{1, \ldots, N^P\}$ with $N^P = 160$ time-steps, while $J_{\text{TTS}}^{\text{Alg}}$, Alg= {NLP-RGDM, LA-RGDM, SC-RGDM, SC & NLP-RGDM}, denote the objective values obtained from the solution of each approach.

Tables 2 and 3 illustrate the execution time and optimality gap of the three approaches for five scenarios of increasing demand (i.e., 2000, 3000, 4000, 5000, and 6000 veh/h) for $T_s = 30$ s, $N^C = 1$ and $N^P = 15$, respectively. Execution times refer to the total time needed to solve the problems associated with one MPC step update. From the results, it can be observed that the SC & NLP-RGDM and SC-RGDM approaches provide almost identical results with the SC & NLP-RGDM approach providing slightly better solutions. Moreover both approaches yield 3- 6 and 1-2 times smaller optimality gap compared to NLP-RGDM and LA-RGDM in all considered cases. In terms of execution speed, the per iteration execution times of NLP-RGDM, SC & NLP-RGDM, LA-RGDM, and SC-RGDM range between 9 - 95 s, 27 - 73 s 0.9- 1.2 s, and 6.5 - 7.1 s, respectively. This means that SC-RGDM runs about an order of magnitude faster than NLP-RGDM and an order of magnitude slower than LA-RGDM. Even though LA-RGDM executes faster than SC-RGDM, both approaches are suitable for real-time applications with the SC-RGDM approach achieving better results.

Table 4 investigates the effect of the prediction horizon size on the execution time of the three RGDM approaches for two scenarios of demand 4000 and 5000 veh/h. Considering both scenarios, the execution time of LA-RGDM and SC-RGDM grows linearly to the prediction horizon, while NLP-RGDM experiences a dramatic growth of execution time for increasing prediction horizon size. More specifically, the execution speed of NLP-RGDM is 2-3 orders of magnitude slower than SC-RGDM when the demand is equal to 4000 veh/h; for the higher demand scenario, the execution speed of NLP-RGDM is even higher. Similarly to the results of Table 2, SC-RGDM is about an order of magnitude slower than LA-RGDM as it sacrifices execution speed to achieve better optimality bounds; however, both

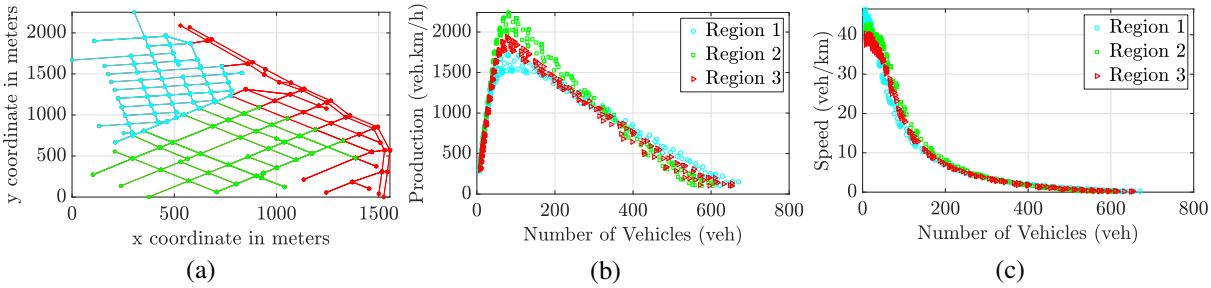


Figure 8: (a) The simulated network consisting of an area of Downtown San Francisco; (b) the production MFD of each region; (c) the speed MFD of each region.

approaches are suitable for real-time applications.

### *4.2. Microscopic simulations*

In this section, we investigate the performance of the proposed methodologies using microscopic simulations. Specifically, we investigate the ability of the SC-RGDM and LA-RGDM traffic control approaches to perform well under significant modelling uncertainty due to the discrepancy between microscopic and macroscopic traffic dynamics.

#### *4.2.1. Setup*

For the microscopic simulation we consider an area of the urban network of Downtown San Francisco. The area under investigation is a 2.5 square miles non-signalized area which consists of 143 road junctions and 319 single-lane road segments with lengths varying from 100 m to 400 m. A similar area has also been used by Aboudolas and Geroliminis (2013) which provide a detailed breakdown of the network into 3 homogeneous regions (i.e., $|\mathcal{R}| = 3$), as illustrated in Figure 8(a) (regions are denoted with different colours). In this setting, we have chosen to evaluate the performance of the proposed SC-RGDM approach as it can offer reliable, fast and close-to-optimal results.

The SUMO microscopic simulator (Behrisch et al., 2011) has been used to create traffic within the network, considering the Wiedemann car-following model (Higgs et al., 2011) with model parameters: vehicle length 5 m, maximum speed 15 m/s, acceleration 2.5 m/s$^2$, deceleration 4.5 m/s$^2$, driver reaction time 0.5 s, minimum gap distance 2.5 m, and simulation time-step 0.1 s. All results are averaged over ten (10) Monte Carlo simulations due to the stochastic nature of SUMO.

The following results assume that all drivers adhere to control actions (e.g., split ratios and waiting times) without any deviation (100% driver compliance rate). Furthermore, all state measurements used in each MPC iteration are provided from SUMO, assuming that all vehicles can communicate their position and destination to the traffic controller. The SC-RGDM and LA-RGDM approaches are compared against the SP strategy where all vehicles follow their shortest time paths in which drivers can change their route (reroute) with probability $p = 0.25$. In SUMO, the option to reroute vehicles is enabled to ensure that vehicles can use the best possible path, considering the current and recent traffic states (Behrisch et al., 2011).

#### *4.2.2. MFD Fitting*

To evaluate our approach at a microscopic level, we first have to determine the MFD of each considered region. For this purpose, a 2-hour SUMO simulation scenario was executed using the SP strategy. For this scenario, the input flow was initially set to 2000 veh/h for the first half-hour and incrementally increased by 500 veh/h for the next three 30-minute periods. Fig. 8(b) depicts the total network production (veh·km/h) as a function of the total number of vehicles in each region (i.e., MFD). Similarly, Fig. 8(c) depicts the identified speed-density relation. In both figures, each point corresponds to the moving average of 5 consecutive state measurements taken every 1 minute.

Using the derived data, we can identify the analytical expressions for the flow and speed MFD functions utilizing an optimization based fitting procedure. The developed MFD functions are continuous and continuously differentiable

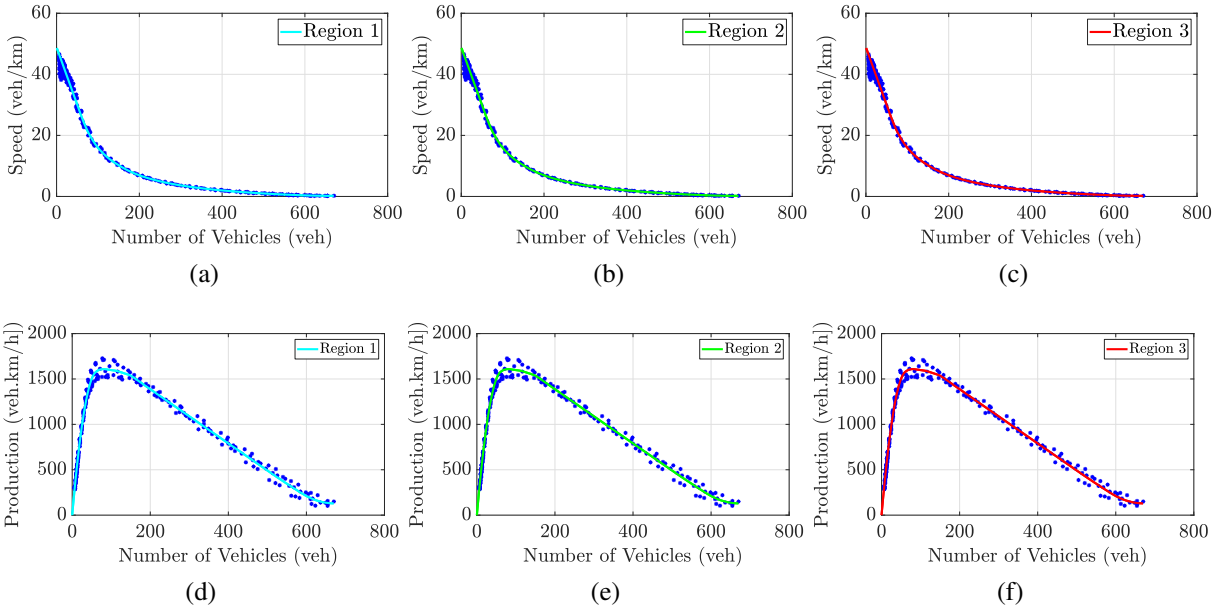


Figure 9: (a)-(c) the fitted speed MFD for each region; (d)-(f) the fitted production MFD.

functions constructed from a set of piecewise quadratic polynomials. The fitting method aims to construct MFD functions that fit as close as possible to actual data based on the convex programming methods. Figs. 9 (a)-(c) and (d)-(f) depict the fitted speed and production MFD functions for the three considered regions which are used in the SC-RGDM approach.

*4.2.3. Results*

The performance of SC-RGDM, LA-RGDM and SP is compared for different 2-hour scenarios with demand varying between $1000 - 7000$ veh/h. Note that, the triangular MFD function used for the LA-RGDM approach is approximated using the Triangular MFD approximation method proposed in Appendix B. Figs. 10 and 11 show the average travel times of vehicles and the average number of vehicles that completed their journey within the simulation time as a function of demand. The scattered plots in Figure 10 show the mean travel time of each simulation run, while the dashed lines represent the mean travel time of the 10 simulations for each considered demand. Similarly, the dashed lines in Fig. 11 illustrate the average number of vehicles that managed to complete their journey within the simulation time for each considered demand, while the scattered plots represent the number of vehicles that complete their journey in each simulation run. Both figures illustrate that SC-RGDM and LA-RGDM outperform SP, as they achieve travel times that are close to free-flow conditions, with all vehicles finishing their trip within the simulation time. More specifically, all approaches perform equally well for low demand, ranging from $1000 - 4000$ veh/h, as no congestion occurs. For demand higher than 5000 veh/h, the SP strategy breaks down causing heavy congestion and large travel times. On the contrary, SC-RGDM and LA-RGDM remain equally efficient yielding travel times close to free-flow conditions and enabling all vehicles to finish their journeys. To illustrate their superior performance, notice that for demand equal to 7000 veh/h both approaches yield almost ten times smaller travel times and double trip completions. In that sense, the SC-RGDM approach can maintain shorter travel times that are slightly affected by the increasing demand, with all vehicles reaching their destination within the simulation time.

Furthermore, Fig. 12 illustrates the space-time diagram of the number of vehicles in each region within the SUMO environment when the demand is 7000 veh/h. Comparing the results form Figs. 10 and 12 we can observe that LA-RGDM can achieve slightly better travel times but yields higher waiting times compared with SC-RGDM such that in total requires more time to serve all vehicles within the network. This is expected as LA-RGDM has lower modeling accuracy. To examine the ability of the MFD-based traffic dynamics to approximate the microscopic dynamics, Fig. 13 illustrates the space-time diagram of the number of vehicles in each region assuming MFD-based traffic dynamics

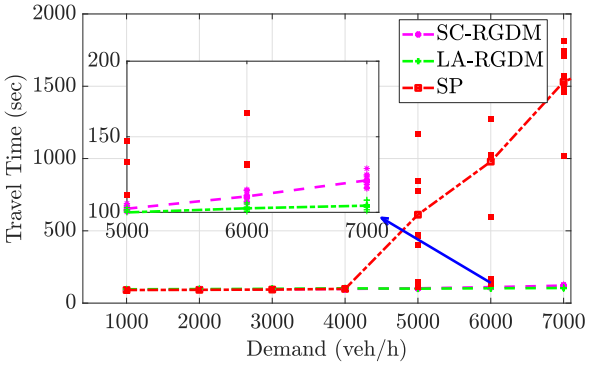


Figure 10: Travel time for different simulation scenarios with varying demand.

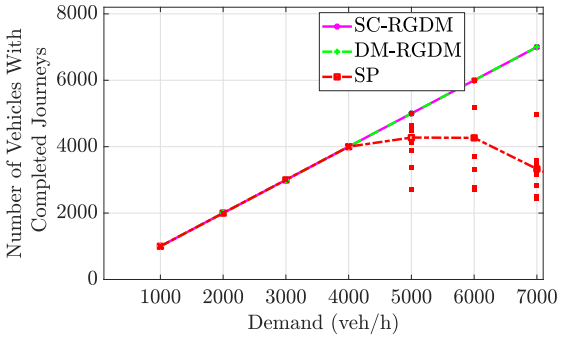


Figure 11: Number of vehicles with completed journeys for different simulation scenarios with varying demand.

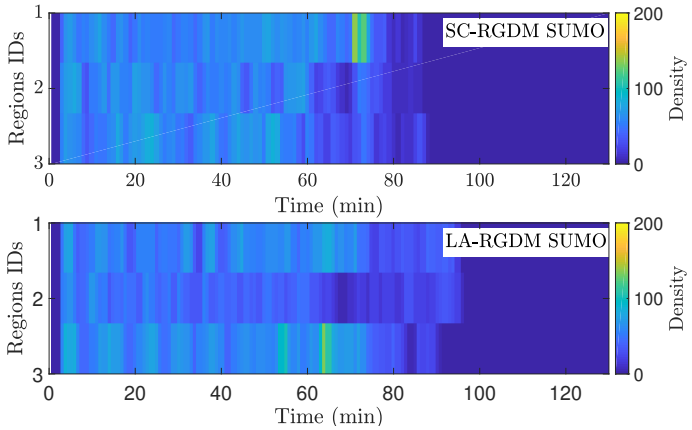


Figure 12: The instantaneous number of vehicles of each region for the SC-RGDM and LA-RGDM schemes observed at each time-step within SUMO simulation.

when the demand is 7000 veh/h. This space-time diagram denotes the perceived densities within a macroscopic simulation. Comparing Figs. 12 and 13 it can be seen that there is a good match both in terms of the observed and perceived densities, as well as the admitted demand in the network. Finally, Fig. 14 illustrates the cumulative number of vehicles that request to enter the network compared to the number of vehicles that are admitted into the network from both approaches when the demand is 7000 veh/h. The figure shows that the LA-RGDM allows a lower number of vehicles to enter due to modeling inaccuracies.

## 5. Discussion

The utilization of macroscopic traffic models has become increasingly popular in modern traffic management methodologies. These models are capable of capturing the collective behavior of traffic flows at a network level, making them more effective in managing traffic compared to microscopic models. One of the fundamental concepts utilized in these models is the Macroscopic Fundamental Diagram (MFD), which simplifies traffic dynamics by representing them as a function of density. Recent studies have demonstrated that MFD-based models can significantly enhance the efficiency of traffic management strategies. One of their main advantages is their simplicity in modeling, which enables the development of MPC frameworks. As a result, these models can aid in the development of more effective and robust traffic management strategies, which can significantly reduce congestion and improve the overall travel experience.

While significant advances have been made in MFD-based traffic management, studies have indicated that their

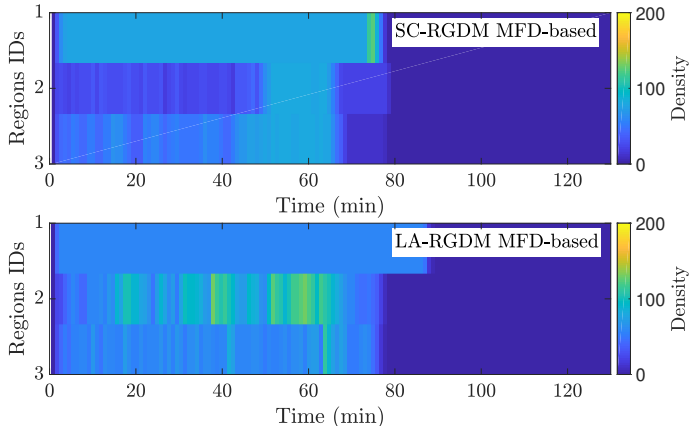


Figure 13: The instantaneous number of vehicles of each region for the SC-RGDM and LA-RGDM scheme observed at each time-step assuming MFD-based traffic dynamics.

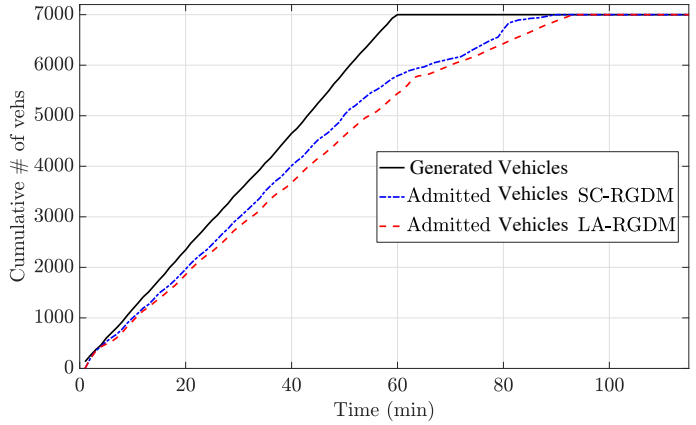


Figure 14: The cumulative number of vehicles that request to enter (*Generated Vehicles*) and the number of vehicles that are actually admitted into the network (*Admitted Demand*) over time.

efficiency is heavily reliant on the specific MFD shape considered. Optimal performance of different traffic management strategies may require varying MFD shapes Ambuhl et al. (2020). This dependence on specific MFD shapes may limit the applicability of real-time traffic management approaches. Furthermore, MFD-based traffic management schemes face another significant challenge. Despite the simplified model, the resulting traffic dynamics are still non linear, leading to non convex and non linear traffic management problems. This non linearity makes it challenging to design efficient and robust traffic management strategies that can account for a wide range of traffic scenarios.

To address the above limitations, this work introduces an MPC approach that can address the challenging problem of jointly managing demand and guiding routes without relying on a specific MFD shape. Our approach considers the demand for vehicles wishing to use the network and the current state of the network, to regulate the departure times of vehicles and identify which multi-region route to follow in order to minimize the total time spent in the network. Since the resulting model still relies on nonlinear traffic dynamics, this study proposes two solution approaches that can approximate the original problem with linear programs, able to provide high-quality and accurate control decisions in real-time. The first approach is a successive convexification procedure that constructs convex sets for all nonlinearities while tightening the discrepancy between the original nonlinear problem and the approximation scheme in successive iterations. The second approach approximates the generalized MFD shape with a triangular MFD shape and solves the resulting linear problem. Macroscopic simulation results indicate that the two approaches have a trade-off between solution quality and execution speed, with the successive convexification approach yielding better quality solutions

and the linear approximation approach faster execution time. A detailed comparison with a state-of-practice MPC nonlinear solver indicates that the proposed solution approaches yield significantly better results in terms of solution quality and execution speed. In particular, this work shows that the proposed methodologies are one-to-two orders of magnitude faster and result in 3-5 times smaller optimality gap. Moreover, simulation results show that our proposed methodologies can be employed for the real-time control of urban areas as both approaches can derive high-quality control actions for the next 20-30 time intervals within 7-12 seconds.

Based on the findings of our research, we have identified three main advantages of our proposed approach. Firstly, our approach delivers high-quality results in terms of both solution quality and execution speed. Simulation results have demonstrated that both of our proposed approaches outperform the solutions obtained from a standard non-linear solver in terms of execution time and solution quality. Specifically, our approaches can offer significant reductions in execution time (more than 30 times) while maintaining, or even improving, the quality of the obtained solutions. These findings highlight the effectiveness and efficiency of our proposed approach in managing traffic flow in real-time scenarios. Secondly, our approach provides global optimality bounds, which enable us to obtain lower and upper bound solutions on the global optimum of the problem. Our simulation results have shown that the upper bound solution can achieve tight bounds over the lower bound solution, indicating that the provided upper bound solution is highly accurate, with their optimality gap being below 10% and 3% for the LA-RGDM and SC-RGDM, respectively. Thirdly, our approach is highly generalizable and can be applied to other traffic management problems, such as perimeter control. This is a crucial feature as the solution methodologies proposed can be adapted for other traffic management strategies. Additionally, our simulation results demonstrate that our proposed approach can alleviate congestion, despite the discrepancy between the actual model and the approximation scheme used within each solution approach. Furthermore, the proposed successive convexification approach has been validated through micro-simulation results, confirming its suitability for real-life traffic management scenarios. Our approach has been shown to provide high-accuracy control decisions in real-time, emphasizing its practicality and effectiveness. Overall, the proposed solution methodology represents a promising solution to the challenges faced by MFD-based traffic management schemes, with the potential to significantly improve the efficiency and effectiveness of traffic management strategies. Microsimulations demonstrate that our methodology can effectively manage traffic demand at a higher level, leading to reduced congestion and improved overall traffic flow.

In conclusion, our proposed methodologies offer an efficient and effective solution for the joint route guidance and demand management problem for multi-region networks with traffic dynamics defined by generalized shaped MFDs, with potential applications in real-time traffic management for large-scale urban areas.

## 6. Conclusions

This work investigates joint route guidance and demand management for multi-region networks with traffic dynamics defined according to generalized shaped MFDs. In this context, a model predictive control framework is formulated yielding a nonlinear nonconvex problem which is challenging to solve with standard solvers. To tackle this problem, our work proposes two solution approaches that approximate the original problem with linear programs. The first approach develops a successive convexification procedure which constructs convex sets to all nonlinearities while tightening traffic state bounds in successive iterations. The second approach approximates generalized with triangular MFDs and solves the resulting linear problem.

Future research will develop custom-made variations of the proposed successive convexification and linear approximation solution approaches for different traffic control strategies. Furthermore, we aim to develop robust and stochastic model predictive control approaches for regional route guidance and demand management that account for measurement noise and modelling uncertainties.

## Acknowledgements

This work has been supported by the European Union's Horizon 2020 research and innovation programme under grant agreement No 739551 (KIOS CoE) and the Government of the Republic of Cyprus through the Directorate General for European Programmes, Coordination and Development.

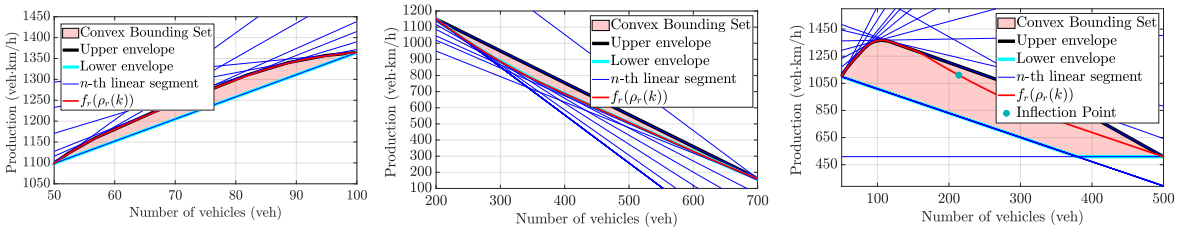


Figure A.15: Depending on the density range and the properties R1 to R5, $f_r(\rho_r(\tau))$ may be: (a) concave, (b) convex, and (c) concave in the range $[\rho_r^l(\tau), \rho_r^I]$ and convex in the range $[\rho_r^I, \rho_r^u(\tau)]$.

## Appendix A. Outer approximation of MFD functions

Appendix A describes the procedure to construct convex *outer approximations* of the generalized flow and speed MFDs under density box constraints. In general terms, given a constraint set of the form $\mathcal{S} = \{(x, y) \mid y = \phi(x),\ x^l \leq x \leq x^u\}$, with $\phi(x)$ being a nonlinear function, the task is to construct a convex polyhedral set defined as $\mathcal{S}^C = \{(x, y) \mid y \leq \widehat{a}_i x + \widehat{b}_i,\ i = 1, 2, ..., \widehat{N},\ y \geq \breve{a}_j x + \breve{b}_j\ j = 1, 2, ..., \breve{N},\ x^l \leq x \leq x^u\}$ such that $\mathcal{S}^C \supseteq \mathcal{S}$. Notice that set $S^C$ has two constraint sets. The first, constructs an upper envelope of $\phi(x)$ in the range $x^l \leq x \leq x^u$ using piecewise linear segments $\widehat{a}_i x + \widehat{b}_i$ for $i = 1, 2, ..., \widehat{N}$, while the second constructs a lower envelope of $\phi(x)$ in the range $x^l \leq x \leq x^u$ using piecewise linear segments $\breve{a}_j x + \breve{b}_j$, for $j = 1, 2, ..., \breve{N}$. Note that in the following section for the sake of notational simplicity we drop index $r$ and $\tau$.

### *A.1. Flow MFD Outer Approximation*

First, let us describe the procedure for the flow-density MFD, i.e., $q = f(l)$, $\rho^l \leq \rho \leq \rho^u$. Here the task is to construct a convex outer approximation set $\mathcal{S}^q$, defined as

$$\mathcal{S}^q = \{(q, \rho) \,|\, \rho^l \leq \rho \leq \rho^u \text{ and } q \leq \widehat{a}_n \rho + \widehat{b}_n, n \in \widehat{\mathcal{N}}^q,\ q \geq \breve{a}_n \rho + \breve{b}_n,\ n \in \breve{\mathcal{N}}^q\},$$

where $\breve{\mathcal{N}}^q = \{1, ..., \breve{N}^q\}$ and $\widehat{\mathcal{N}}^q = \{1, ..., \widehat{N}^q\}$ denote the sets of piecewise linear segments comprising the lower and upper envelopes that approximate $f(\rho)$ from below and above when $\rho^l \leq \rho \leq \rho^u$.

Depending on the density range and the properties of the $f(\rho)$ function which may be: (i) concave if $\rho^u \leq \rho^I$, (ii) convex if $\rho^l \geq \rho^I$, and (iii) concave in the range $[\rho^l, \rho^I]$ and convex in the range $[\rho^I, \rho^u]$, with $\rho^I$ serving as the *inflection point*, i.e., the point at which the function $f(\rho)$ changes from concave to convex. Next, we examine how to deal with each of the three cases.

*Case 1: $f(\rho)$ is concave*

In general, to construct $\mathcal{S}^q$ we need to derive the lower and upper envelopes of the curve $f(\rho)$ from piecewise linear segments. The lower envelope is comprised of one linear segment that passes from points $(\rho^l, f(\rho^l))$ and $(\rho^u, f(\rho^u))$; hence, we have that $\breve{\mathcal{N}}^q = 1$ with

$$\breve{a}_1 = \frac{f(\rho^u) - f(\rho^l)}{\rho^u - \rho^l}, \tag{A.1}$$

$$\breve{b}_1 = f(\rho^l) - a_1^l \rho^l. \tag{A.2}$$

To construct the upper envelope of $f(\rho)$, we create linear segments that are tangent to $f(\rho)$ at non-uniform density points, starting from $\rho^l$. Assuming that the $i$th tangent point is $\widehat{\rho}_i$, the parameters of the $i$th linear segment $\widehat{a}_i$ and $\widehat{b}_i$

are

$$\widehat{a}_i = f'(\widehat{\rho}_i), \tag{A.3}$$

$$\widehat{b}_i = f(\widehat{\rho}_i) - a_i^l \widehat{\rho}_i. \tag{A.4}$$

Then, the next tangent point $\widehat{\rho}_{i+1}$ is selected such that

$$\widehat{a}_i \widehat{\rho}_{i+1} + \widehat{b}_i - f(\breve{\rho}_{i+1}) = \delta, \tag{A.5}$$

where $\delta > 0$ is a small predefined constant. In other words, we create a new tangent line at the point where the difference between the current tangent line and the curve grow to $\delta$. This procedure is repeated until the upper density bound is reached, as depicted in Fig. A.15 (a).

*Case 2: $f(\rho)$ is convex*

Here the reverse procedure is followed: the upper envelope is a single linear segment produced from points $(\rho^l, f(\rho^l))$ and $(\rho^u, f(\rho^u))$, while the lower envelope is constructed from tangent lines similar to Case 1, as illustrated in Fig. A.15 (b).

*Case 3: $f(\rho)$ is concave in $[\rho^l, \rho^I]$ and convex in $[\rho^I, \rho^u]$*

The tangent linear segment procedure, followed in Cases 1 and 2, is used for the construction of the upper and lower envelopes with some changes in the procedure. To construct the upper envelope, we generate tangent lines from lower to higher densities starting from $\rho^l$ until $\rho^I$. The procedure stops when a generated tangent line with parameters $\tilde{a}_{\widehat{n}}$ and $\tilde{b}_{\widehat{n}}$, with index $\widehat{n} = \widehat{N}^q$, falls below the curve $f(\rho)$ at the upper value of the density, $\rho^u$, i.e.

$$\widehat{\xi} = \tilde{a}_{\widehat{n}} \rho^u + \tilde{b}_{\widehat{n}} - f(\rho^u) \leq 0.$$

To re-establish feasibility of the outer approximation we shift the particular line upwards by $-\widehat{\xi}$ yielding

$$\tilde{a}_{\widehat{n}} \rho + \tilde{b}_{\widehat{n}} - \widehat{\xi} = \tilde{a}_{\widehat{n}} (\rho - \rho^u) + f(\rho^u). \tag{A.6}$$

Notice that now the curve and the $\widehat{n}$th tangent line coincide at $\rho = \rho^u$. The new line segment has parameters $\widehat{a}_{\widehat{n}} = \tilde{a}_{\widehat{n}}$ and $\widehat{b}_{\widehat{n}} = f(\rho^u) - \tilde{a}_{\widehat{n}} \rho^u$. In case no such tangent line is found, the procedure stops when the density point $\rho^I$ is reached.

A similar approach is taken to construct the lower envelope with two differences. First, the procedure proceeds from higher to lower densities starting from $\rho^u$ until $\rho^I$. Second, the procedure stops when a generated tangent line with parameters $\tilde{a}_{\breve{n}}$ and $\tilde{b}_{\breve{n}}$, with index $\breve{n} = \breve{N}^q$, is above $f(\rho)$ at the lower value of the density $\rho^l$. In this case the line is shifted downwards yielding line parameters $\breve{a}_{\breve{n}} = \tilde{a}_{\breve{n}}$ and $\breve{b}_{\breve{n}} = f(\rho^l) - \tilde{a}_{\breve{n}} \rho^l$.

Since the function $f(\rho)$ is unimodal, the horizontal line segment that connects points $(\rho^l, \varphi)$ and $(\rho^u, \varphi)$, with $\varphi = \min\{f(\rho^l), f(\rho^u)\}$, is also part of the lower envelope, as depicted in Fig. A.15 (c).

*A.2. Speed MFD Outer Approximation*

To obtain a convex bounding set for the speed MFD relationship we follow the same procedure with Case 2 for the flow MFD because function $g(\rho)$ is convex.

## Appendix B. Triangular MFD approximation

Appendix B describes the procedure to approximate a generalized flow MFD function $f(\rho)$ with a triangular MFD $f^T(\rho)$. Similarly with Appendix A in the following section we drop index $r$ and $\tau$ for notational simplicity.

The triangular MFD $f^T(\rho)$ consists of two linear segments for the free-flow and congested regimes which are defined by Eq.(33). Hence, the task at hand is to identify the optimal values of $\delta_1, \delta_2$ and $\delta_3$ that provide the best fit

between $f(\rho)$ and $f^T(\rho)$ in the least-squares sense. The triangular MFD is allowed to be discontinuous at the critical density $\rho^C$ such that our fitting problem can be decomposed into the following two distinct optimization problems for the free-flow $[0, \rho^C]$ and congested regimes $[\rho^C, \rho^J]$, respectively.

$$\underset{\delta_1}{\text{Minimize}} \int_0^{\rho^C} \Big(\delta_1 \rho - f(\rho)\Big)^2 d\rho \tag{B.1}$$

$$\underset{\delta_2, \delta_3}{\text{Minimize}} \int_{\rho^C}^{\rho^J} \Big(\delta_2 \rho + \delta_3 - f(\rho)\Big)^2 d\rho \tag{B.2}$$

The fitting problems (B.1) and (B.2) aim to minimize the area between the generalized MFD function $f(\rho)$ and each of the two linear segments of $f^T(\rho)$ in the least-squares sense, assuming that both functions have the same critical density. Integrating out variable $\rho$ yields

$$\underset{\delta_1}{\text{Minimize}}\ \delta_1^2 \alpha_1 + \delta_1 \alpha_2 + \alpha_3 \tag{B.3}$$

$$\underset{\delta_2, \delta_3}{\text{Minimize}}\ \delta_2^2 \alpha_4 + \delta_3^2 \alpha_5 + \delta_2 \delta_3 \alpha_6 + \delta_2 \alpha_7 + \delta_3 \alpha_8 + \alpha_9 \tag{B.4}$$

where $\alpha_i$, $i = \{1, ..., 9\}$, are constants given by $\alpha_1 = (\rho^C)^3/3$, $\alpha_2 = -2\int_0^{\rho^C} \rho f(\rho) d\rho$, $\alpha_3 = \int_0^{\rho^C} f^2(\rho) d\rho$, $\alpha_4 = (\rho^J)^3/3 - (\rho^C)^3/3$, $\alpha_5 = \rho^J - \rho^C$, $\alpha_6 = (\rho^J)^2 - (\rho^C)^2$, $\alpha_7 = -2\int_{\rho^C}^{\rho^J} \rho f(\rho) d\rho$, $\alpha_8 = -2\int_{\rho^C}^{\rho^J} f(\rho) d\rho$, and $\alpha_9 = \int_{\rho^C}^{\rho^J} f^2(\rho) d\rho$. Formulations (B.3) and (B.4) are unconstrained optimization problems whose optimal solution can be found by setting the derivative of the objective functions of (B.3) and (B.4) with respect to the corresponding variables to zero and solving the resulting linear equation systems. Performing this procedure yields the optimal values for $\delta_1$, $\delta_2$ and $\delta_3$ as

$$\begin{aligned}
\delta_1 &= -\frac{\alpha_2}{2\alpha_1}, \\
\delta_2 &= \frac{-2\alpha_5\alpha_7 + \alpha_8\alpha_6}{-\alpha_6^2 + 4\alpha_4\alpha_5}, \\
\delta_3 &= \frac{-\delta_2\alpha_6 - \alpha_8}{2\alpha_5}.
\end{aligned}$$

## Appendix C. Symbols, notation and parameters

Table (C.5) provides an overview of the symbols, notation and parameters used in this work to facilitate the reader's understanding of the paper.

| Notation | Definition | Units |
|---|---|---|
| $\mathcal{R}$ | Set of all regions in the network | - |
| $\mathcal{O}$ | Set of origin regions of different flows | - |
| $\mathcal{D}$ | Set of destination regions of different flows | - |
| $\mathcal{J}_r$ | Set of neighbouring regions directly accessible from region $r \in \mathcal{R}$ | - |
| $\mathcal{S}^q_{rk}$ | Convex bounding set of flow-density MFD relationship $q_r(k) = f_r(\rho_r(k))$ of region $r \in \mathcal{R}$ at time-slot $k$ | - |
| $\mathcal{S}^v_{rk}$ | Convex bounding set of speed-density MFD relationship $v_r(k) = g_r(\rho_r(k))$ of region $r \in \mathcal{R}$ at time-slot $k$ | - |
| $\breve{\mathcal{N}}^q_{rk}$ | Set of piecewise linear segments that approximate $q_r(k)$ from below | - |
| $\hat{\mathcal{N}}^q_{rk}$ | Set of piecewise linear segments that approximate $q_r(k)$ from above | - |
| $\breve{\mathcal{N}}^v_{rk}$ | Set of piecewise linear segments that approximate $v_r(k)$ from below | - |
| $\hat{\mathcal{N}}^v_{rk}$ | Set of piecewise linear segments that approximate $v_r(k)$ from above | - |
| $\mathcal{L} = \{1, ..., L\}$ | Set of all segments of the density and speed MFDs | - |
| $\tau$ | Time-step index | - |
| $T_s$ | Duration of each time-slot | $s$ |
| $L_r$ | The total length of region $r \in \mathcal{R}$ | m |
| $l_r$ | The average trip length of vehicles inside region $r \in \mathcal{R}$ | m |
| $\rho^J_r$ | Jam density of region $r \in \mathcal{R}$ | veh/km |
| $\rho^C_r$ | Critical density of region $r \in \mathcal{R}$ | veh/km |
| $D^{MAX}_{od}$ | Maximum possible demand that can physically enter region $o \in \mathcal{O}$ towards $d \in \mathcal{D}$ | veh |
| $\rho^I_r$ | Inflection density point of region $r \in \mathcal{R}$ | veh/km |
| $v^{MAX}_r$ | Maximum speed in the region $r \in \mathcal{R}$ | km/h |
| $\gamma_{rjd}$ | Ratio of vehicles that move from $r \in \mathcal{R}$ to $d \in \mathcal{D}$ through neighbouring region $j \in J_r$ | - |
| $C^{\text{MAX}}_{rj}$ | Maximum inter-boundary capacity from region $r \in \mathcal{R}$ to region $j \in J_r$ | veh/h |
| $\rho_r(k)$ | Density of region $r \in \mathcal{R}$ at time-slot $k$ | veh/km |
| $q_r(k)$ | Intended outflow of region $r \in \mathcal{R}$ at time-slot $k$ | veh/h |
| $v_r(k)$ | Average speed of region $r \in \mathcal{R}$ at time-slot $k$ | km/h |
| $v^f_r$ | Free-flow speed of region $r \in \mathcal{R}$ assuming a triangular shaped MFD | km/h |
| $P_r(k)$ | Production of region $r \in \mathcal{R}$ at time-slot $k$ | veh.km/h |
| $n_r(k)$ | The number of vehicles in $r \in \mathcal{R}$ at time-slot $k$ | veh |
| $f_r(\rho_r(k))$ | Asymmetric unimodal function describing the flow-density MFD relationship in region $r \in \mathcal{R}$ | veh/h |
| $f^T_r(\rho_r(k))$ | Triangular function describing the approximated flow-density MFD relationship in region $r \in \mathcal{R}$ | veh/h |
| $g_r(\rho_r(k))$ | Monotonically decreasing function describing the speed-density relationship in region $r \in \mathcal{R}$ | km/h |
| $d_{od}(k)$ | Instantaneous external demand requesting to enter from $o \in \mathcal{O}$ towards $d \in \mathcal{D}$ | veh |
| $\tilde{d}_{od}(k)$ | Admitted external demand from $o \in \mathcal{O}$ towards $d \in \mathcal{D}$ | veh |
| $D_{od}(k)$ | Cumulative external demand requesting to enter from $o \in \mathcal{O}$ towards $d \in \mathcal{D}$ | veh |
| $\rho_{rd}(k)$ | Density in region $r \in \mathcal{R}$ towards $d \in \mathcal{D}$ | veh/km |
| $q_{rd}(k)$ | Intended transfer flow from $r \in \mathcal{R}$ to $d \in \mathcal{D}$ | veh/h |
| $q_{rjd}(k)$ | Intended transfer flow from $r \in \mathcal{R}$ to $d \in \mathcal{D}$ through neighbouring region $j \in J_r$ | veh/h |
| $C_{rj}(\rho_j(k))$ | Inter-boundary capacity from region $r \in \mathcal{R}$ to region $j \in J_r$ | veh/h |
| $\tilde{q}_{rjd}(k)$ | Actual transfer flow from $r \in \mathcal{R}$ to $d \in \mathcal{D}$ through neighbouring region $j \in J_r$ | veh/h |
| $S^a(k)$ | Cumulative number of vehicles requesting to enter the network | veh |
| $S^b(k)$ | Cumulative number of vehicles successfully arriving at their destination | veh |
| $\rho^l_r(k)$ | Upper-bound of $\rho_r(k)$ | veh/km |
| $\rho^u_r(k)$ | Lower-bound of $\rho_r(k)$ | veh/km |
| $\rho^l_{rd}(k)$ | Upper-bound of $\rho_{rd}(k)$ | veh/km |
| $\rho^u_{rd}(k)$ | Lower-bound of $\rho_{rd}(k)$ | veh/km |
| $v^l_r(k)$ | Upper-bound of $v_r(k)$ | km/h |
| $v^u_r(k)$ | Lower-bound of $v_r(k)$ | km/h |
| $\hat{\rho}_r(k)$ | State estimate for the density of region $r \in \mathcal{R}$ | veh/km |

Table C.5: The symbols, notation and parameters used in this work.

## References


Aboudolas, K., Geroliminis, N., 2013. Perimeter and boundary flow control in multi-reservoir heterogeneous networks. Transportation Research Part B: Methodological 55, 265–281.

Ambuhl, L., Loder, A., Bliemer, M.C., Menendez, M., Axhausen, K.W., 2020. A functional form with a physical meaning for the macroscopic fundamental diagram. Transportation Research Part B: Methodological 137, 119–132. URL: https://www.sciencedirect.com/science/article/pii/S0191261517310123, doi:https://doi.org/10.1016/j.trb.2018.10.013. advances in Network Macroscopic Fundamental Diagram (NMFD) Research.

Arnott, R., Small, K., 1994. The economics of traffic congestion. American Scientist 82, 446–455.

Behrisch, M., Bieker, L., Erdmann, J., Krajzewicz, D., 2011. SUMO-Simulation of Urban MObility-an overview, in: The Third International Conference on Advances in System Simulation, pp. 55–60.

Bellocchi, L., Geroliminis, N., 2020. Unraveling reaction-diffusion-like dynamics in urban congestion propagation: Insights from a large-scale road network. Scientific Reports 10, 1–11.

Biegler, L.T., Zavala, V.M., 2009. Large-scale nonlinear programming using IPOPT: An integrating framework for enterprise-wide dynamic optimization. Computers & Chemical Engineering 33, 575–582.

Daganzo, C.F., 2007. Urban gridlock: macroscopic modeling and mitigation approaches. Transportation Research Part B: Methodological 41, 49–62.

Genser, A., Kouvelas, A., 2020. Optimum route guidance in multi-region networks: A linear approach, in: 99th Annual Meeting of the Transportation Research Board, pp. 20–30.

Geroliminis, N., Daganzo, C.F., 2008. Existence of urban-scale macroscopic fundamental diagrams: Some experimental findings. Transportation Research Part B: Methodological 42, 759–770.

Geroliminis, N., Sun, J., 2011. Properties of a well-defined macroscopic fundamental diagram for urban traffic. Transportation Research Part B: Methodological 45, 605–617.

Groot, N., De Schutter, B., Hellendoorn, H., 2012. Integrated model predictive traffic and emission control using a piecewise-affine approach. IEEE Transactions on Intelligent Transportation Systems 14, 587–598.

Gurobi Optimization Inc., 2016. Gurobi Optimizer Reference Manual. URL: http://www.gurobi.com.

Haddad, J., Geroliminis, N., 2012. On the stability of traffic perimeter control in two-region urban cities. Transportation Research Part B: Methodological 46, 1159–1176.

Hajiahmadi, M., Haddad, J., Schutter, B.D., Geroliminis, N., 2015. Optimal hybrid perimeter and switching plans control for urban traffic networks. IEEE Transactions on Control Systems Technology 23, 464–478. doi:10.1109/TCST.2014.2330997.

Hajiahmadi, M., Knoop, V.L., Schutter, B.D., Hellendoorn, H., 2013. Optimal dynamic route guidance: A model predictive approach using the macroscopic fundamental diagram, in: 16th International IEEE Conference on Intelligent Transportation Systems (ITSC 2013), pp. 1022–1028. doi:10.1109/ITSC.2013.6728366.

Higgs, B., Abbas, M., Medina, A., 2011. Analysis of the wiedemann car following model over different speeds using naturalistic data, in: Procedia of RSS Conference, pp. 1–22.

Ji, Y., Geroliminis, N., 2012. On the spatial partitioning of urban transportation networks. Transportation Research Part B: Methodological 46, 1639–1656.

Keyvan-Ekbatani, M., Kouvelas, A., Papamichail, I., Papageorgiou, M., 2012. Exploiting the fundamental diagram of urban networks for feedback-based gating. Transportation Research Part B: Methodological 46, 1393–1403.

Kouvelas, A., Saeedmanesh, M., Geroliminis, N., 2017. Enhancing model-based feedback perimeter control with data-driven online adaptive optimization. Transportation Research Part B: Methodological 96, 26–45. URL: https://www.sciencedirect.com/science/article/pii/S019126151630710X, doi:https://doi.org/10.1016/j.trb.2016.10.011.

Kouvelas, A., Saeedmanesh, M., Geroliminis, N., 2019. Linear parameter varying model predictive control for multi-region traffic systems, in: 98th Annual Meeting of the Transportation Research Board, TRB. pp. 19–39.

Kumarage, S., Yildirimoglu, M., Ramezani, M., Zheng, Z., 2021. Schedule-constrained demand management in two-region urban networks. Transportation Science 55, 857–882.

Leclercq, L., Ladino, A., Becarie, C., 2021. Enforcing optimal routing through dynamic avoidance maps. Transportation Research Part B: Methodological 149, 118–137.

Luten, K., 2004. Mitigating Traffic Congestion: The role of demand-side strategies. Technical Report. U.S. Department of Transport, Federal Highway Administration.

Macfarlane, J., 2019. When apps rule the road: The proliferation of navigation apps is causing traffic chaos. it's time to restore order. IEEE Spectrum 56, 22–27.

Maciejowski, J.M., 2002. Predictive control: with constraints. Pearson Education.

Mahmassani, H.S., 1998. Dynamic traffic simulation and assignment: Models, algorithms and application to atis/atms evaluation and operation, in: Operations Research and Decision Aid Methodologies in Traffic and Transportation Management. Springer, pp. 104–135.

McCormick, G.P., 1976. Computability of global solutions to factorable nonconvex programs: Part I: Convex underestimating problems. Mathematical Programming 10, 147–175.

Menelaou, C., Timotheou, S., Kolios, P., Panayiotou, C., 2019. Joint route guidance and demand management for multi-region traffic networks, in: 2019 18th European Control Conference (ECC), IEEE. pp. 2183–2188.

Menelaou, C., Timotheou, S., Kolios, P., Panayiotou, C., 2021a. A convex reformulation solution approach for the joint perimeter control and route guidance problem, in: 2021 IEEE International Intelligent Transportation Systems Conference (ITSC), pp. 2541–2546. doi:10.1109/ITSC48978.2021.9564404.

Menelaou, C., Timotheou, S., Kolios, P., Panayiotou, C.G., 2020. Joint route guidance and demand management using generalized mfds∗∗this work has been supported by the european union's horizon 2020 research and innovation programme under grant agreement no 739551 (kios coe), the government of the republic of cyprus through the directorate general for european programmes, coordina-

tion and development and through the research promotion foundation (project: Culture/br-ne/0517/14). IFAC-PapersOnLine 53, 15023–15028. URL: https://www.sciencedirect.com/science/article/pii/S2405896320326331, doi:https://doi.org/10.1016/j.ifacol.2020.12.2002. 21th IFAC World Congress.

Menelaou, C., Timotheou, S., Kolios, P., Panayiotou, C.G., 2021b. Joint route guidance and demand management for real-time control of multi-regional traffic networks. IEEE Transactions on Intelligent Transportation Systems , 1–14doi:10.1109/TITS.2021.3077870.

Menelaou, C., Timotheou, S., Kolios, P., Panayiotou, C.G., Polycarpou, M.M., 2019. Minimizing traffic congestion through continuous-time route reservations with travel time predictions. IEEE Transactions on Intelligent Vehicles 4, 141–153. doi:10.1109/TIV.2018.2886684.

Papageorgiou, M., 1990. Dynamic modeling, assignment, and route guidance in traffic networks. Transportation Research Part B: Methodological 24, 471 – 495. doi:https://doi.org/10.1016/0191-2615(90)90041-V.

Papageorgiou, M., Diakaki, C., Dinopoulou, V., Kotsialos, A., Wang, Y., 2003. Review of road traffic control strategies. Proceedings of the IEEE 91, 2043–2067.

Saeedmanesh, M., Kouvelas, A., Geroliminis, N., 2021. An extended kalman filter approach for real-time state estimation in multi-region mfd urban networks. Transportation Research Part C: Emerging Technologies 132, 103384. URL: https://www.sciencedirect.com/science/article/pii/S0968090X21003831, doi:https://doi.org/10.1016/j.trc.2021.103384.

Sirmatel, I.I., Geroliminis, N., 2018. Economic model predictive control of large-scale urban road networks via perimeter control and regional route guidance. IEEE Transactions on Intelligent Transportation Systems 19, 1112–1121. doi:10.1109/TITS.2017.2716541.

Sirmatel, I.I., Geroliminis, N., 2021. Stabilization of city-scale road traffic networks via macroscopic fundamental diagram-based model predictive perimeter control. Control Engineering Practice 109, 104750. URL: https://www.sciencedirect.com/science/article/pii/S0967066121000277, doi:https://doi.org/10.1016/j.conengprac.2021.104750.

Sirmatel, I.I., Tsitsokas, D., Kouvelas, A., Geroliminis, N., 2021. Modeling, estimation, and control in large-scale urban road networks with remaining travel distance dynamics. Transportation Research Part C: Emerging Technologies 128, 103157. URL: https://www.sciencedirect.com/science/article/pii/S0968090X21001753, doi:https://doi.org/10.1016/j.trc.2021.103157.

Tsitsokas, D., Kouvelas, A., Geroliminis, N., 2023. Two-layer adaptive signal control framework for large-scale dynamically-congested networks: Combining efficient max pressure with perimeter control. Transportation Research Part C: Emerging Technologies 152, 104128. URL: https://www.sciencedirect.com/science/article/pii/S0968090X23001171, doi:https://doi.org/10.1016/j.trc.2023.104128.

Yildirimoglu, M., Ramezani, M., 2020. Demand management with limited cooperation among travellers: A doubly dynamic approach. Transportation Research Part B: Methodological 132, 267–284. URL: https://www.sciencedirect.com/science/article/pii/S019126151831138X, doi:https://doi.org/10.1016/j.trb.2019.02.012. 23rd International Symposium on Transportation and Traffic Theory (ISTTT 23).

Yildirimoglu, M., Ramezani, M., Geroliminis, N., 2015. Equilibrium analysis and route guidance in large-scale networks with mfd dynamics. Transportation Research Part C: Emerging Technologies 59, 404–420.

Yildirimoglu, M., Sirmatel, I.I., Geroliminis, N., 2018. Hierarchical control of heterogeneous large-scale urban road networks via path assignment and regional route guidance. Transportation Research Part B: Methodological 118, 106 – 123. doi:https://doi.org/10.1016/j.trb.2018.10.007.